Praise Worthy Prize

International Review of Biophysical Chemistry (I.RE.BI.C.), Vol. 4, N. 5
ISSN 2038 - 0321 *October 2013*

Ultrafast Spectroscopic Studies on the Interaction of a Potential Food Carcinogen with Biologically Relevant Macromolecules

Soma Banerjee, Siddhi Chaudhuri, Samir Kumar Pal

Abstract – *Benzo[a]pyrene (BP), a potential carcinogen in a class of pyrene derivatives shows interesting photophysics including very sharp vibronic structures in the emission spectrum. A detail spectroscopic study on the close interaction of the carcinogenic molecule with other biologically relevant macromolecules through ultrafast energy/charge transfer reactions is the motive of the present review. Firstly, we present our picosecond resolved studies on the Förster resonance energy transfer (FRET) from various vibronic bands in BP, showing strong dependency on the spectral overlap of an energy acceptor in a confined environment. Our study on the dipolar interactions between BP and different acceptors ethidium (Et), acridine orange (AO) and crystal violet (CV) at the surface of a model anionic micelle reveals the Förster distance (R_0) and the rate of energy transfer to be dependent on the individual spectral overlap of the vibronic bands of BP with the absorption spectra of different energy acceptors. The differential behaviour of the vibronic bands is compared with that of different dyes (quantum dots; QDs) in a 'dye-blend' (mixture) under FRET to an energy acceptor. Such comparison of the FRET of QDs with that of BP, not only confirms independent nature of dipolar interaction of the vibronic bands with other organic molecules, the use of deconvolution technique in the interpretation of the donor-acceptor (D-A) distance has also been justified. We have also shown that consideration of differential FRET from vibronic bands of BP and from the QDs in the 'dye-blend' is equally acceptable in the theoretical frameworks including 'Infelta-Tachiya' model and D-A distribution analysis in the nano-environments. While such energy transfer reactions act as "spectroscopic ruler" to measure the distance between two sites on a macromolecule, reactions involving electron transfer (ET)/charge transfer (CT) and reactive oxygen species (ROS) play a pivotal role in carcinogenesis and cancer biochemistry. The review further emphasizes our studies on UVA radiation induced ET reaction as one of the key aspects of BP in the presence of a wide variety of molecules covering organic para-benzoquinone (BQ), biological macromolecules like calf-thymus DNA (CT-DNA), human serum albumin (HSA) protein and inorganic zinc oxide (ZnO) nanorods (NRs). Steady-state and picosecond-resolved fluorescence spectroscopy have been used to monitor such ET reactions. Physical consequences of BP association with CT-DNA have been investigated through temperature-dependent circular dichroism (CD) spectroscopy. The temperature-dependent steady-state, picosecond-resolved fluorescence lifetime and anisotropy studies reveal the effect of temperature on the perturbation of such ET reactions from BP to biological macromolecules, highlighting their temperature-dependent association. Furthermore, the electron donating property of BP has been corroborated by measuring wavelength-dependent photocurrent in a BP-anchored ZnO NR-based photodevice, offering new physical insights for the carcinogenic study of BP.*

Keywords: *Benzo[A]Pyrene (BP), Vibronic Fine Structures, Förster Resonance Energy Transfer (FRET), Nanoscopic Micelle, Quantum Dots Blend, Femtosecond Resolved Vibrational Cooling, UVA Radiation Induced Electron Transfer (ET) Reaction, Temperature-Dependent Picosecond-Resolved Fluorescence of BP, Temperature-Dependent Binding of BP to DNA and Protein, Zinc Oxide Nanorod (Zno NR) Fabricated Photodevice*

Nomenclature

R_0	Förster distance
κ^2	Orientation factor
n	Refractive index
Q_D	Quantum yield
$J(\lambda)$	Overlap integral
E	Energy transfer efficiency
r	Distance between donor and acceptor
P_n^*	Micelle containing n quencher molecules and one excited probe
P_n	Micelle containing n quencher molecules

Manuscript received and revised September 2013, accepted October 2013

k_q Rate constant for quenching of an excited probe in a micelle containing one quencher molecule
k_0 Total decay constant of an excited probe in absence of quencher in micelle
m Mean number of quenchers in a micelle
$[A]$ Concentration of quencher molecule in the aqueous phase
k_+ Rate constant for entry of a quencher molecule in a micelle
k_- Rate constant for exit of a quencher molecule from a micelle containing one quencher molecule
$P^*(t)$ Total concentration of excited probes in a micelle at time t
K_{eq} Equilibrium constant
$P(r)$ Distance distribution function

I. Introduction

Pyrene molecules belonging to a class of polyaromatic hydrocarbons (PAHs) have several appealing photophysical properties which make them suitable for use as effective fluorescence probes [1]-[4]. One of those properties is the sensitivity of their spectral parameters, such as change in vibronic structure (especially intensity ratios of first and third vibronic bands) to the change of the environment [5].

The effects of temperature and solute-solvent interactions on the various vibronic fine structures in the emission spectra of pyrene class of molecules have been well explored [2], [6]-[7] and reveal the differential perturbation of the individual vibronic bands. Benzo[*a*]pyrene (BP), one of the well-known pyrene derivatives and a potential carcinogen to which humans are most frequently exposed [8], exhibits differential shifts of its individual vibronic structures as a function of the refractive index of the surrounding solvent [6]. BP is a by-product of grilled foods [9] and tobacco [10] and fuel combustion [11]-[12] and has long been linked to various human cancers, particularly lung and skin. Though there have been extensive studies on the environmental effects on the steady-state florescence spectrum of pyrene [2], solvatochromism of BP manifested through their excitation and emission peak shifts in a wide variety of solvents [6], the effects of different solvents on the excited state lifetime at the different vibronic bands of such molecules, highlighting the consequence of solvent dipole/dielectric constant on the non-radiative rates are less attended.

Another important aspect is the dipolar interaction of the pyrene class of dyes with other molecules manifested in Förster resonance energy transfer (FRET).

The differential behavior of the individual vibronic bands, in the emission spectra of pyrene and its derivatives, in response to change in temperature [7], polarity and refractive index [6] of the host solvent is well known while reports on such behavior of these bands while undergoing dipolar interactions with different molecules is sparse in the literature.

FRET, which is also known as "spectroscopic ruler" [13]-[15], is very often used to measure the distance between two sites on a macromolecule [16]. As pyrene and its derivatives are known to interact with biological macromolecules [6], [17], FRET can serve as an efficient tool for the investigation of the biomolecular recognition of these molecules. In one of the earlier studies [18], attempts to use FRET from pyrene class of molecules to perylene have been made for nucleic acid assays under homogeneous solution conditions using steady-state spectroscopy.

In another recent study [19], FRET has been used as a tool for the detection of PAH's antibody binding using a hydroxyl derivative of BP as a FRET donor and sulforhodamine B as the energy acceptor employing both steady-state and time resolved spectroscopy. However, investigation of the vibronic bands under dipolar coupling, was beyond the scope of the studies. It has also to be noted that estimation of D-A distance from steady-state FRET studies is found to be inconclusive [20]. In this regard exploration of the excited state dynamics of the different vibronic bands of BP while undergoing dipolar interactions with different molecules in a biologically relevant environment has immense importance and is the motive of our present review.

While FRET processes have significant contribution in the exploration of ultrafast dynamical pathways involved in non-radiative energy migration in various biomolecules, electron transfer (ET) or charge transfer (CT) processes have pivotal role in carcinogenesis and cancer biochemistry [21]. The accepted hypothesis for carcinogens is that they are first converted to electrophilic metabolites which react covalently with the nucleophilic DNA.

Such DNA adducts are the ultimate molecular lesion leading to the activation of oncogenes and ultimately giving rise to neoplasia [22]. Earlier studies [23] indicate the significance of one electron oxidation as a possible primary step in the chemical carcinogenesis of BP. ET reactions are well known for their importance in DNA damage [24] and recent findings suggest the role of ultrafast ET in inducing single strand and double strand breaks in DNA through reductive DNA damage [25].

Previous reports investigating BP-DNA complexes through fluorescence and triplet flash photolysis techniques have proposed that majority of the fluorescence in these complexes originates from BP bound to GC-GC intercalation sites [26]. Such conclusions are supported by the relative quenching efficiencies of BP by mononucleosides dissolved in aqueous ethanol mixtures suggesting 2'-deoxythymidine as an efficient quencher compared to cytidine, 2'-deoxyguanosine and -adenosine.

Furthermore, it has also been reported [26] that the fluorescence of BP in aqueous BP-DNA complexes gets strongly quenched upon the addition of Ag^+ ions which bind predominantly to guanosine in DNA, validating the fact that fluorescence of BP in BP-DNA complexes originates from GC sites.

However, the study does not preclude the possibility of BP binding at AT rich sites. The same study reports shorter lifetime of BP in DNA complexes compared to that in degassed benzene suggesting strong fluorescence quenching of BP upon complexation with DNA.

BP fluorescence quenching by nucleoside solutions shows no association between the quencher and BP in the ground state, while a short lived charge transfer complex is formed when an excited state BP collides with a nucleoside [26]. In such charge transfer complexes, determination of the electron donor and acceptor is based on the relative ionization potentials and electron affinities of the two molecules forming the complex.

The ionization potentials of the aromatic hydrocarbons are generally lower than the nitrogenous bases [26] and calculations indicate that pyrimidines are better electron acceptors than purines.

Earlier studies [27] report that genotoxic carcinogens not only interact with DNAs but also with proteins. In this regard, serum proteins are particularly important because hepatocytes are not only the cells in which serum proteins are synthesized but also the cells in which most xenobiotic metabolism, including microsomal oxidations which activate carcinogens, takes place. Among serum proteins, serum albumin being abundant and because of its role as a carrier of fatty acids, endobiotics and xenobiotics, there is a high probability that it will bind and form covalent adducts with ultimate carcinogens. There have been extensive studies on the adduct formation of BP with serum albumin [28]-[29] yet the information regarding the ET reaction between the two are sparse in the present literature. Moreover, it is of great interest to discuss the effect of temperature on such ET reaction between BP and biological macromolecules like DNA and protein.

Apart from chemical carcinogens, ionizing radiations play a significant role in the induction of cancer [30]-[31]. Certain radiations like UVA are also known to cause DNA damage through ET in the presence of certain photosensitizers [32]. Earlier studies have shown how coexposure to BP and UVA induces double strand breaks (DSBs) in DNA, in both cell-free system (in vitro) and cultured Chinese hamster ovary (CHO-K1) cells [33]-[34], resulting in phototoxicity and photocarcinogenesis. A singlet oxygen scavenger sodium azide (NaN_3) effectively showed inhibition in the production of DSBs, suggesting singlet oxygen is the principal ROS generated by BP and UVA both in vitro and in vivo [34]. It has also been suggested that the mechanism of DNA damage by BP in presence of UVA differs in cell and cell-free systems. In spite of such extensive reports, the exploration of photophysics lying behind the co-exposure of DNA to BP and UVA radiation is less explored in the literature to the best of our knowledge.

Recently, an ultrasensitive photoelectrochemical immunoassay comprising bifunctional gold nanoparticles modified with PAH antigen and horseradish peroxidise (HRP) on nanostructured TiO_2 electrode decorated with antibodies has been proposed as a means to quantify PAH, based on the changes in photocurrent with respect to the control (without PAH) [35].

However, studies emphasizing the application of nanostructure [36] based photodevices in the detection of ET reaction, where flow of electrons can be directly monitored in the form of photocurrent, are sparse in the literature.

In short, our present review makes an attempt to explore the ultrafast processes associated with the carcinogen BP for better understanding of its photophysical as well as carcinogenic properties.

II. Methodology

II.1. Steady-State and Time Resolved Studies

Steady-state absorption and emission were measured with Shimadzu Model UV-2450 spectrophotometer and Jobin Yvon Model Fluoromax-3 fluorimeter respectively.

All picosecond transients were measured by using commercially available (Edinburgh Instrument, UK) picosecond-resolved time correlated single photon counting (TCSPC) setup (instrument response function, IRF of 80 ps) using 375 excitation laser source (from Picoquant, Germany). Fluorescence from the sample was detected by a photomultiplier after dispersing through a double grating monochromator.

For all transients the polarizer in the emission side was adjusted to be at 54.7^o (magic angle) with respect to the polarization axis of the excitation beam. In order to get reasonably good signal to noise ratio, all the TCSPC experiments were carried out with at least 5000 counts. The femtosecond-resolved fluorescence was measured using a femtosecond upconversion setup (FOG 100, CDP), the sample was excited at 375 nm (0.5 nJ per pulse), using the second harmonic of a mode-locked Ti-sapphire laser with an 80 MHz repetition rate (Tsunami, Spectra Physics), pumped by 10 W Millennia (Spectra Physics). The fundamental beam is frequency doubled in a nonlinear crystal (1mm BBO, $\theta = 25^o$, $\phi = 90^o$).

The fluorescence emitted from the sample is up-converted in a nonlinear crystal (0.5 mm BBO, $\theta = 10^o$, $\phi = 90^o$) using a gate pulse of the fundamental beam. The upconverted light is dispersed in a double monochromator and detected using photon counting electronics. A cross-correlation function obtained using the Raman scattering from water displayed a full width at half maximum (FWHM) of 165 femtosecond (fs).

II.2. Förster Resonance Energy Transfer (FRET)

In order to estimate the Förster resonance energy transfer (FRET) efficiency of the donor (BP) to the different acceptors (Et, AO and CV) and hence to determine distances (r) of donor-acceptor pairs, we have followed the methodology described in chapter 13 of ref[37].

The Förster distance (R_0) is given by:

$$\frac{R_0}{\text{Å}} = 0.211\left[\kappa^2 n^{-4} Q_D J(\lambda)\right]^{1/6} \quad (1)$$

where (κ^2) is a factor describing the relative orientation in space of the transition dipoles of the donor and acceptor.

The value of the orientation factor (κ^2) is calculated from the equation:

$$\kappa^2 = \left(cos\,\theta_T - 3cos\,\theta_D\, cos\,\theta_A\right)^2 \quad (2)$$

where θ_T is the angle between the emission transition dipole of the donor and absorption transition dipole of the acceptor and θ_D and θ_A are the angles between these dipoles and the vector joining the donor and acceptor[37]. In the micellar system, the donor and acceptor molecules can be bound simultaneously without any restriction on the relative orientation of their transition dipole moments. Thus, the orientation parameter (κ^2) can be taken as 0.667[37].

Moreover, since the sixth root is taken to calculate the distance, variation of κ^2 from the value for random orientation (κ^2 = 2/3) to that for parallel dipolar orientation (κ^2 = 1) or to that for head-to-tail parallel transition dipoles (κ^2 = 4) the calculated distance can be in error by no more than 35%[37].

The refractive index (n) of the medium was measured and found to be 1.3 which is apparent since the space separating the donor and acceptor consists of the hydrophobic tails (alkyl chain) of the SDS micelle and the refractive index of similar alkanes like pentane, hexane, heptane, dodecane etc varies between 1.30 and 1.42. Q_D, the quantum yield of the donor in the absence of acceptor, was calculated according to the equation [38]:

$$Q = Q_R\left(\frac{I}{I_R}\right)\left(\frac{OD_R}{OD}\right)\left(\frac{n^2}{n_R^2}\right) \quad (3)$$

where Q and Q_R are the quantum yield of BP in SDS micelle and reference (Hoechst 33258 in SDS), I and I_R are the integrated fluorescence intensities of BP and reference, OD and OD_R are the optical densities of BP and reference at the excitation wavelength and n and n_R are the refractive indices of BP and reference solutions.

The absolute quantum yield of Hoechst 33258 [16] in SDS was taken to be 0.54.

Refractive indices of the solutions were measured by using Rudolph J357 automatic refractometer.

The quantum yield of BP in SDS micelle has been found to be near unity and relative Q_D of BP in SDS micelle at different emission peaks has been calculated upon deconvoluting the BP emission at its emission peaks around 410, 430 and 455 nm and has been calculated to be 0.45, 0.43 and 0.10 respectively.

$J(\lambda)$, the overlap integral, which expresses the degree of spectral overlap between the donor emission and the acceptor absorption, is given by:

$$J(\lambda) = \frac{\int_0^\infty F_D(\lambda)\varepsilon(\lambda)\lambda^4 d(\lambda)}{\int_0^\infty F_D(\lambda) d(\lambda)} \quad (4)$$

where $F_D(\lambda)$ is the fluorescence intensity of the donor in the wavelength range of λ to $\lambda + d\lambda$ and is dimensionless. $\varepsilon(\lambda)$ is the extinction coefficient (in M^{-1} cm^{-1}) of the acceptor at λ. If λ is in nm, then $J(\lambda)$ is in units of M^{-1} cm^{-1} nm^4. Once the value of R_0 is known, the donor-acceptor distance (r) can be calculated using the formula:

$$r^6 = \left[R_0^6\left(1-E\right)\right]/E \quad (5)$$

where, E is the efficiency of energy transfer. The efficiency (E) is calculated from the average lifetimes of the donor in the absence and presence of acceptors (τ_D and τ_{DA}):

$$E = 1 - \frac{\tau_{DA}}{\tau_D} \quad (6)$$

II.3. 'Infelta-Tachiya' Model (Kinetic Model)

The decay of excited BP probes in a micelle may be described by the following kinetic model [39]:

$$P_n^* \xrightarrow{k_0} P_n \quad (7)$$

$$P_n^* \xrightarrow{nk_q} P_n \quad (8)$$

where P_n^* and P_n stand for a micelle containing n quencher molecules with and without an excited probe, respectively. k_0 is the total decay constant of the excited state in absence of a quencher.

k_q is the rate constant for quenching of an excited probe in a micelle containing one quencher molecule. In this kinetic model, it is assumed that the distribution of the number of quenchers attached to one micelle follows a Poisson distribution,[40] namely:

$$p(n) = \left(m^n / n!\right) exp(-m) \quad (9)$$

where m is the mean number of quenchers in a micelle:

$$m = k_+\left[A\right]/k_- \quad (10)$$

where k_+ is the rate constant for entry of a quencher molecule into a micelle, while k_- is the rate constant for exit of a quencher molecule from a micelle containing one quencher molecule. "A" stands for a quencher molecule in the aqueous phase.

Based upon the above model, the equation for the total concentration $P^*(t)$ of excited probes at time t is given by [39]:

$$P^*(t) = P^*(0)\cdot \cdot exp\left[\begin{array}{l} -\left(k_0 + \frac{k_0 k_+ [A]}{k_- + k_q}\right)t + \\ -\frac{k_q^2 k_+ [A]}{k_-\left(k_- + k_q\right)^2}\left\{1 - exp\left[-\left(k_- + k_q\right)t\right]\right\} \end{array}\right] \quad (11)$$

If k_- is much smaller than k_q, Eq. (11) reduces to:

$$P^*(t) = P^*(0)\,exp\left\{-k_0 t - m\left[1 - exp\left(-k_q t\right)\right]\right\} \quad (12)$$

The observed fluorescence transients were fitted using a nonlinear least squares fitting procedure (software SCIENTIST™) to a function $\left(X(t) = \int_0^t E(t')P(t-t')dt'\right)$ comprising of the convolution of the instrument response function (IRF) $\left(E(t)\right)$ with exponential:

$$\left(P^*(t) = P^*(0)\,exp\left\{-k_0 t - m\left[1 - exp\left(-k_q t\right)\right]\right\}\right)$$

The purpose of this fitting is to obtain the decays in an analytic form suitable for further data analysis.

In case of QDs, along with the acceptor CV, there exist some unidentified traps that further cause quenching of the lifetime of excited QD probe, which are also taken into account. If the distribution of the number of unidentified traps around the donor QDs follows a Poisson distribution with the average number (m_t), the decay curves of the excited state of QDs in toluene in absence and presence of CV are described by [41]:

$$P^*(t,0) = P^*(0)\,exp\left\{-k_0 t - m_t\left[1 - exp\left(-k_{qt} t\right)\right]\right\} \quad (13)$$

$$P^*(t,m) = P^*(0)\,exp\left\{\begin{array}{l} -k_0 t - m_t\left[1 - exp\left(-k_{qt} t\right)\right] + \\ -m\left[1 - exp\left(-k_q t\right)\right] \end{array}\right\} \quad (14)$$

where the quenching rate constant (k_{qt}) by unidentified traps may be different from that (k_q) by acceptor CV.

II.4. Distance Distribution in Donor-Acceptor Systems

Distance distribution between donor and acceptor was estimated according to the procedure described in the literature [37], [42]. The observed fluorescence transients of the donor BP molecules in absence of acceptor (Et) in the micelle were fitted using a nonlinear least-squares fitting procedure (software SCIENTIST) to the following function:

$$I_D(t) = \int_0^t E(t')P(t'-t)dt' \quad (15)$$

which comprises the convolution of the instrument response function (IRF) ((*E*(*t*)) with exponential ($P(t) = \sum_i \alpha_{Di}\,exp\left(-t/\tau_{Di}\right)$).

The convolution of the distance distribution function *P*(*r*) in the fluorescence transients of donor in presence of acceptor in the system under studies (micelle) is estimated using the same software (SCIENTIST) in the following way.

The intensity decay of donor-acceptor pair, spaced at a distance '*r*', is given by:

$$I_{DA}(r,t) = \sum_i \alpha_{Di}\,exp\left[-\frac{t}{\tau_{Di}} - \frac{t}{\tau_{Di}}\left(\frac{R_0}{r}\right)^6\right] \quad (16)$$

and the intensity decay of the sample considering *P*(*r*) is given by:

$$I_{DA}(t) = \int_{r=0}^{\infty} P(r)\,I_{DA}(r,t)\,dr \quad (17)$$

where *P*(*r*) consist of the following terms:

$$P(r) = \frac{1}{\sigma\sqrt{2\pi}}\,exp\left[-\frac{1}{2}\left(\frac{\bar{r}-r}{\sigma}\right)^2\right] \quad (18)$$

In this equation $\bar{r}$ is the mean of the Gaussian with a standard deviation of σ. Usually distance distributions are described by the full width at half maxima. This half width is given by hw= 2.354σ. Similar procedure has been followed to find the distance distribution of donor QDs and acceptor CV in toluene.

II.5. Preparation of BP-ZnO Based Photodevice

Detailed processes for the hydrothermal growth of the single crystalline ZnO NRs are described in our previous reports [43]-[44]. Briefly, a 1 mM Zinc acetate dehydrate, $Zn(CH_3COO)_2{\cdot}2H_2O$ (Merck), solution in isopropanol was used to prepare the ZnO seed layer on a fluorinated tin oxide (FTO) substrate followed by annealing in air at 350°C for 5 h. A 20 mM aqueous solution of zinc nitrate hexahydrate, $Zn(NO_3)_2{\cdot}6H_2O$ (Sigma-Aldrich), and hexamethylenetetramine, $C_6H_{12}N_4$ (Aldrich), was used as a precursor solution for ZnO NR growth and the seeded FTO substrates were dipped into it at 90°C for 40 h. As-grown ZnO NRs on the FTO substrates were then taken out from the precursor solution and rinsed with deionized (DI) water several times to remove unreacted residues from the substrate.

Finally, the substrates with ZnO NRs were annealed at 350°C for 1 h in air and dipped into 3.9 mM DMSO solution of BP and kept in the dark. After 24 h the photoelectrodes were removed from the BP solution and rinsed several times with DMSO in order to remove weakly adsorbed dye molecules.

Since BP does not have any functional group through which it can bind to inorganic NRs, the only possible way of binding is physisorption.

Platinized FTO glass was used as a counter electrode where a thin platinum layer was deposited on FTO-coated glass substrates by thermal decomposition of platinum chloride, $H_2PtCl_6 \cdot H_2O$ (Fluka), at 385°C for 15 min.

The counter electrode was then placed on top of the photoelectrode and a single layer of 50 μm thick surlyn 1702 (Dupont) was used as a spacer between the two electrodes. The photodevices were then sealed and filled with the liquid electrolyte, consisting of 0.5 M lithium iodide (LiI), 0.05 M iodine (I_2) and 0.5 M 4-tert-butylpyridine (TBP) in acetonitrile (ACN), through two small holes (ϕ= 1 mm) drilled on the counter electrode.

Finally, the two holes were sealed by surlyn to prevent electrolyte leakage. A control ZnO NR photoelectrode without BP was also prepared for comparison.

II.6. Data Analysis

Curve fitting of observed fluorescence transients was carried out using a nonlinear least-square fitting procedure to a function $\left(X(t) = \int_0^t E(t') R(t-t') dt' \right)$ comprised of convolution of the IRF ($E(t)$) with a sum of exponentials $\left(R(t) = A + \sum_{i=1}^{N} B_i e^{-t/\tau_i} \right)$ with pre-exponential factors (B_i), characteristic lifetimes (τ_i), and a background (A).

Relative concentration in a multiexponential decay is expressed as:

$$c_n = \frac{B_n}{\sum_{i=1}^{N} B_i} \times 100$$

The average lifetime (amplitude-weighted) of a multiexponential decay [37] is expressed as:

$$\tau_{av} = \sum_{i=1}^{N} c_i \tau_i$$

After the deconvolution, obtained time constants which are one-fourth of the IRF may be reliably reported within the signal-to-noise ratio of the fluorescence transients.

III. Results and Discussions

III.1. A Potential Carcinogenic Pyrene Derivative Under FRET to Various Energy Acceptors in Nanoscopic Environments

In this section we have discussed excited state fluorescence relaxation dynamics of BP in a number of solvents with various dipole moments/refractive index. We have compared the relaxation dynamics of the vibronic bands in the solvents in order to investigate the effect of solvent polarity, dipole moment on the excited state lifetime of BP at various emission wavelengths.

Steady-state and time resolved experiments of BP in the anionic micellar solutions confirmed the location of the probe BP.

In order to study the dipolar interaction of BP with another organic dye, we have monitored FRET [45] from BP to a well-characterized acceptor (and potential mutagen [46]) ethidium (Et), which selectively binds to the surface of the micelle [39], [47]. Steady-state and picosecond resolved studies on the FRET between BP and Et from various vibronic bands have been analyzed using conventional and differential methods.

The differential method introduced in this study relies on the individual spectral overlap of the vibronic bands with the absorption spectrum of acceptor Et and found to be more realistic for the estimation of D-A distance. We have also studied FRET between BP and acridine orange (AO) in the micelle to establish generality of the technique for the estimation of D-A distance.

Unambiguous confirmation of the introduced technique is revealed from the FRET from BP to crystal violet [48] (CV) in the nano-environments. CV is observed to offer significant and negligibly small spectral overlap with the band 3 (emission peak at 455 nm) and band 1 (emission peak at 410 nm), respectively.

The differential behaviour of the vibronic bands of BP undergoing dipolar interaction with energy acceptors in the micellar solution has been compared with that of different dyes in a model system of ‘dye-blend’ (mixture of dyes) representing different electronic systems undergoing FRET with CV in toluene. In this regard, three different quantum dots (QDs), QD480, QD570 and QD625 having emission maxima at 480, 570 and 625 nm, respectively have been considered as the components of the ‘dye-blend’. Theoretical framework employing well known ‘Infelta-Tachiya model’ [39], [49] and D-A distance distribution analysis have also been considered in our study in order to further establish the validity of the introduced differential technique of FRET calculation [50].

III.1.1. Effect of Different Solvents on the Excited State Lifetime of Benzo[a]pyrene (BP)

Normalized absorption and emission spectra of BP in various solvents are presented in Fig. 1(a). Solvent dependent shifting of both the absorption and the fluorescence spectra of BP is in close agreement with earlier studies suggesting solvent sensitive changes in the ground as well as the excited state electronic properties of BP.

The picosecond resolved fluorescence transients of BP in different solvents are shown in Fig. 1(b) and the multiexponential fitting parameters are tabulated in Table I. Fig. 1(b) and Table I indicate that the lifetime of BP varies with solvents without much deviation at the

different vibronic fine structures. As evident from Table I, BP shows biexponental decays with time constants of 2-5 ns and 12-20 ns in all the solvents. It has to be noted that the absorption and emission spectra of BP in all the solvents are consistent with those of the monomeric form of BP[6]. No clear correlation of the excited state lifetime with the polarity/proticity of the solvents is evident from the Table I.

For example the lifetime values of BP in DMSO (polar aprotic) and dioxane (non-polar aprotic) are similar. Similarity of lifetime values in ethanol (polar protic) and acetonitrile (polar aprotic) is also noticeable. In an earlier study using steady-state spectroscopy, it has been shown that spectral shifts of the vibronic bands of BP depend on the polarizability (rather dielectric constant) of the host solvents [6]. We have also investigated the polarizability dependence of radiative rate constants of BP in various solvents with different refractive indices.

The excited state lifetime values of BP in various solvents are tabulated in Table II. It is evident from Figs. 2 that the experimental values of radiative rate constants (*kr*) (blue dots) of BP in different solvents are way off from the theoretical estimation (solid line) following different theoretical models [51]. Therefore, a distinct correlation of the spectral shift/lifetime of the vibronic fine structures with the dipole moment/dielectric constant/ refractive index is not evident from our studies and invites more studies, which are motivations of our future works.

However, the excited state photophysics including fluorescence lifetime of BP in various solvents are found to be useful to conclude the location of the probe BP in micro heterogeneous environment. The comparison of the emission spectra and excited state lifetime of BP in dioxane (non-polar and aprotic) with that in the sodium dodecyl sulphate (SDS) micelle (Figure 3) clearly reveals that probe BP prefers to stay in the hydrophobic core of the micelle which is in close agreement with the earlier studies.

III.1.2. Photophysical Characterization of the Excited BP Molecules

Upon excitation with the laser source of 375 nm, the BP molecules are typically excited to S_1, usually to an excited vibrational level. The multiple peaks in the absorption spectrum of BP in SDS solution at 330, 349, 368 and 388 nm, as shown in Fig. 3 are assigned to the individual electronic transitions of BP as reported earlier [52]. The molecular symmetry of BP [52] being C_s allows infinite possible moment directions for electric dipole allowed transitions: perpendicular to the molecular plane (e.g. $\sigma \rightarrow \pi^*$) or along any direction in it ($\pi \rightarrow \pi^*$).

The angles Φ formed by the moments of observed transitions with a specific, well-defined molecular axis in the plane is reported [52] to be 30^o for the electronic transition at 330, 349, 368 and 388 nm.

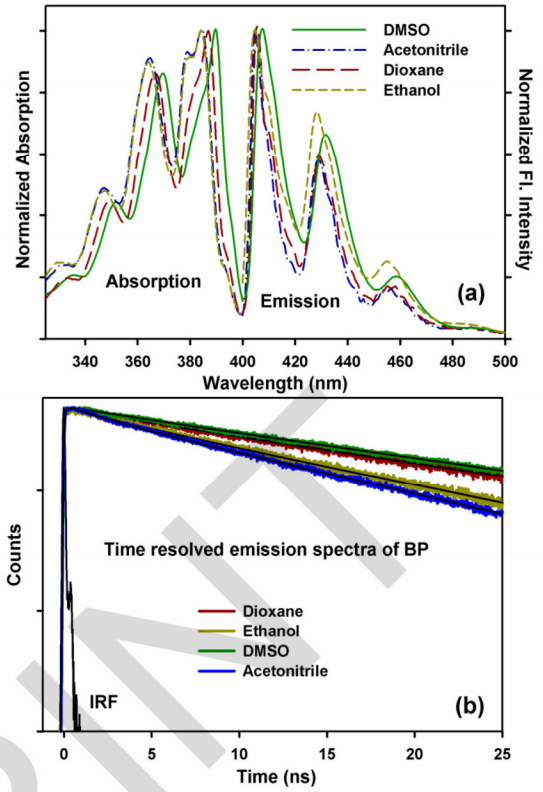

Figs. 1. (a) Normalized absorption and emission spectra of BP in different solvents, DMSO, acetonitrile, dioxane and ethanol and (b) the time resolved fluorescence transients of the same at 410 nm (λ_{em}) upon exciting at 375 nm (λ_{ex}). (Reprinted the colored/modified version of the original Figure in reference [50] with permission from reference [50]. Copyright 2013 WILEY-VCH Verlag GmbH & Co. KGaA, Weinheim)

TABLE I
THE LIFETIME COMPONENTS OF BP AT ITS CHARACTERISTIC EMISSION PEAKS IN VARIOUS SOLVENTS. τ REPRESENTS THE TIME CONSTANT IN NS AND THE NUMBERS IN THE PARENTHESIS REPRESENT RELATIVE CONTRIBUTION OF THE COMPONENT. τ_{AV} REPRESENTS THE AVERAGE LIFETIME IN NS. ERROR ±5%

Sample	Wavelength (nm)	τ_1 (ns)	τ_2 (ns)	τ_{av} (ns)
BP in DMSO	410	2.00 (5%)	20.10 (95%)	19.20
	430	2.00 (10%)	20.10 (90%)	18.30
	455	2.00 (20%)	20.50 (80%)	16.80
BP in acetonitrile	410	2.10 (12%)	12.50 (88%)	11.30
	430	1.80 (14%)	12.60 (86%)	11.10
	455	1.60 (26%)	12.60 (74%)	9.70
BP in dioxane	410	5.00 (9%)	20.30 (91%)	18.90
	430	5.00 (11%)	20.40 (89%)	18.70
	455	5.00 (20%)	20.70 (80%)	17.60
BP in ethanol	410	3.60 (10%)	14.20 (90%)	13.20
	430	3.30 (11%)	14.20 (89%)	13.00
	455	3.30 (20%)	14.00 (80%)	11.90

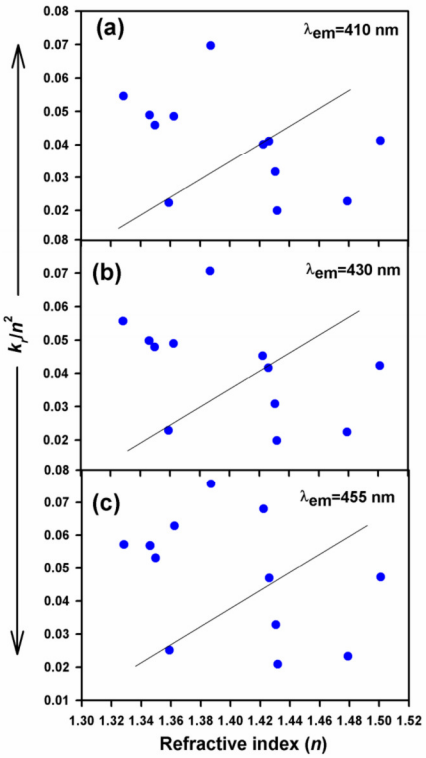

Figs. 2. Plot of k_r/n^2 vs. refractive index (n) of the solvents at different vibronic bands of BP having emission maxima at (a) 410, (b) 430 and (c) 455 nm. k_r represents radiative rate constants of BP. Solid line represents estimation from theoretical models [51] while blue dots are the values obtained from experiments. (Reprinted the colored/modified version of the original Figure in reference [50]with permission from reference [50]. Copyright 2013 WILEY-VCH Verlag GmbH & Co. KGaA, Weinheim)

The orientation factor K_i, the average cosine square of the angle between the moment of transition and the molecular orientation axis has also been reported with a value of 0.56 for the above electronic transitions [52].

An interesting consequence of emission to higher vibrational ground states is that the emission spectrum is typically a mirror image of the absorption spectrum of the $S_0 \rightarrow S_1$ transition (Fig. 3). This similarity occurs because electronic excitation does not greatly alter the nuclear geometry [37]. Fig. 3 upper inset shows the femtosecond resolved fluorescence transient of BP in SDS micelle at 455 nm, upon exciting the probe at 375 nm. The transient can be fitted biexponentially with the time constants of 1.33 ps (61%) and 30 ns (39 %).

The slower component of 30 ns has been obtained from picosecond resolved experiments (see later) and has been fixed in the above fitting.

The faster time constant (1.33 ps) is close to the time constant of ~ 2 ps which is assigned to the vibrational cooling of the S_1 local pyrene state, initially formed with excess vibrational energy [53].

Lower inset of Fig. 3 shows the excitation spectra of BP in SDS micelle which is identical for each vibronic structure, thus, rules out the possibility of accumulation of different excited states.

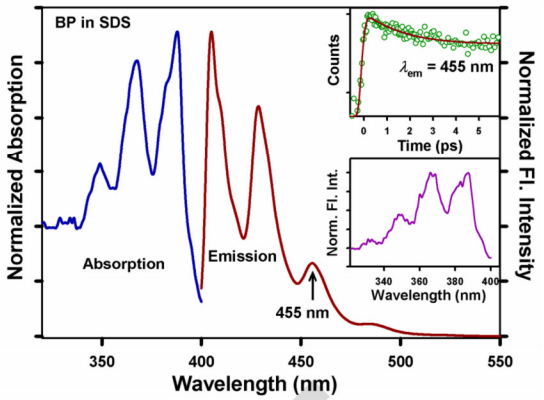

Fig. 3. Normalized absorption and emission spectra of BP in SDS micelle. Lower inset shows the normalized excitation spectrum of the same. Upper inset shows femtosecond resolved fluorescence transient of BP at one of its emission peaks (455 nm) upon excitation at 375 nm. (Reprinted the colored/modified version of the original Figure in reference [50]with permission from reference [50]. Copyright 2013 WILEY-VCH Verlag GmbH & Co. KGaA, Weinheim)

III.1.3. Differential Behaviour of the Vibronic Bands of BP Under FRET

To monitor the characteristic behaviour of different vibronic bands of BP while undergoing dipolar interactions, we employed Förster resonance energy transfer (FRET) studies. For accomplishment of such studies, we have used a well-characterized FRET acceptor ethidium (Et) at the surface of the anionic micelle [39], [47]. Fig. 4(a) shows spectral overlap between the emission spectrum of the BP (donor) and the absorption spectrum of the Et (acceptor) in SDS micelle. At this juncture it is worth mentioning that the FRET analysis considering overall overlap integral (J(λ)) of BP emission with Et absorption spectrum, unable to rationalize following two observations as evident from Figs. 4.

Firstly, different vibronic bands are undergoing different degrees of fluorescence quenching (Fig. 4(c)).

Secondly, the picosecond resolved non-radiative energy transfer rates from various vibronic bands are also found to be significantly different (Figs. 4(d), (e) and (f) and Table IV). The estimated D-A distance with this analysis process also reveals significant fluctuation in the values reported from different vibronic bands.

The above anomaly can easily be taken care if the individual J(λ) for each vibronic band with Et absorption spectrum is considered. The deconvoluted emission spectra of BP at its three well characterized emission peaks at 410, 430 and 455 nm are shown in Fig. 4(b).

Here, it has to be noted that BP monomers also produce a weak emission band at around 480 nm [21] which has not been considered in the present study.

The overlap integral, J(λ), between the deconvoluted emission spectrum of the donor and the absorption spectrum of the acceptor, has been characterized for each vibronic band and the corresponding overlaps are shown in red, green and blue colors for emission maxima at 410,

430 and 455 nm respectively. The corresponding values of J(λ) are tabulated in Table III. The energy transfer takes place from the donor to the acceptor, as indicated by the quenching of fluorescence intensity (Fig. 4(c)) as well as the faster decay (Figs. 4(d), (e) and (f)) of the donor in the donor-acceptor complexes in micelles compared to that of only donor in the micelle. To compare the energy transfer efficiency of the donor from its various vibronic bands, the fluorescence transients of the donor at its different emission peaks, 410, 430 and 455 nm have been monitored in absence and presence of the acceptor Et (Figs. 4(d), e, f and Table IV).

As evident from the Figs. 4(d), (e), (f) and Table IV, the average lifetime of BP at 410, 430 and 455 nm is 29.92, 29.46 and 27.84 ns respectively. The slower component of 30 ns in the fluorescence transients of BP in SDS micelle, as given in Table IV has been confirmed upon repeating the experiments with longer time window of 400 ns. Details of the FRET parameters from various vibronic bands are tabulated in Table III. Here it has to be noted that the vibrational relaxation timescale as observed from our femtosecond resolved experiments is much faster than the energy transfer rates from the vibronic bands.

Thus, FRET is expected to occur after the thermalization process in the excited state. It is clear that the energy transfer efficiency (E) is higher at 455 nm compared to that at 410 nm and consistent with the overlap integral, $J(\lambda)$, between the deconvoluted donor emission at the corresponding wavelengths, with the absorption spectrum of the acceptor (Et), as shown in Figure 4(b). From our time resolved studies the donor-acceptor distance (r) can be estimated to be 1.95±0.08 nm and the fluctuation (0.8 Å) is well within the experimental error limit.

Upon finding the different energy transfer efficiency of the individual vibronic bands of BP undergoing FRET with the acceptor Et molecules, another acceptor acridine orange (AO) has been chosen to find the consistency of such observation.

AO, a cationic dye, is known to interact with SDS micelle through both hydrophobic and electrostatic interactions as the hydrophobic aromatic rings of the AO molecule remain within the hydrophobic core of the SDS micelle, and the charged intracyclic imino group and the two terminal polar amino groups remain outward directed toward the stern layer [54]-[56].

Figs. 5(a) and (b) respectively show the overall and deconvoluted spectral overlap between the emission spectrum of the BP (donor) and the absorption spectrum of the AO (acceptor) in the micelle.

TABLE II
THE FLUORESCENCE LIFETIME COMPONENTS τ_1 AND τ_2 REPRESENT FLUORESCENCE LIFETIMES OF BP IN DIFFERENT SOLVENTS. NUMBERS IN PARENTHESIS SHOW RELATIVE CONTRIBUTION. ERROR ±5%

Solvents	Refractive index (n)	Wavelength (nm)	τ_1 (ns)	τ_2 (ns)	τ_{av} (ns)	k_r (ns^{-1})
DMSO	1.479	410	2.00 (5%)	20.10 (95%)	19.20	0.05
		430	2.00 (10%)	20.10 (90%)	18.30	0.05
		455	2.00 (20%)	20.50 (80%)	16.80	0.06
Acetonitrile	1.346	410	2.10 (12%)	12.50 (88%)	11.30	0.09
		430	1.80 (14%)	12.60 (86%)	11.10	0.09
		455	1.60 (26%)	12.60 (74%)	9.70	0.10
Dioxane	1.4224	410	5.00 (9%)	20.30 (91%)	18.90	0.08
		430	5.00 (11%)	20.40 (89%)	18.70	0.09
		455	5.00 (20%)	20.70 (80%)	17.60	0.14
Ethanol	1.3624	410	3.60 (10%)	14.20 (90%)	13.20	0.09
		430	3.30 (11%)	14.20 (89%)	13.00	0.09
		455	3.30 (20%)	14.00 (80%)	11.90	0.12
Acetone	1.359	410	1.30 (7%)	26.00 (93%)	24.30	0.04
		430	1.00 (9%)	26.00 (91%)	23.70	0.04
		455	1.30 (14%)	24.80 (86%)	21.60	0.05
Benzene	1.5011	410	1.50 (9%)	11.70 (91%)	10.80	0.10
		430	1.40 (11%)	11.60 (89%)	10.50	0.10
		455	1.60 (20%)	11.40 (80%)	9.40	0.11
Cyclohexane	1.4262	410	1.10 (9%)	13.10 (91%)	12.00	0.08
		430	1.10 (11%)	13.20 (89%)	11.80	0.09
		455	1.30 (20%)	12.80 (80%)	10.50	0.10
Diethyl ether	1.3497	410	1.10 (9%)	13.10 (91%)	12.00	0.08
		430	1.20 (11%)	12.80 (89%)	11.50	0.09
		455	1.50 (20%)	12.60 (80%)	10.40	0.10
Dimethyl formamide (DMF)	1.4305	410	0.80 (7%)	16.50 (93%)	15.40	0.07
		430	1.00 (5%)	16.60 (95%)	15.90	0.06
		455	1.30 (9%)	16.30 (91%)	14.90	0.07
Ethylene glycol	1.4318	410	0.70 (9%)	27.00 (91%)	24.50	0.04
		430	0.70 (9%)	27.00 (91%)	24.50	0.04
		455	0.90 (11%)	26.30 (89%)	23.40	0.04
Methanol	1.3284	410	0.70 (11%)	11.60 (89%)	10.40	0.10
		430	0.60 (13%)	11.60 (87%)	10.20	0.10
		455	1.30 (16%)	11.50 (84%)	9.90	0.10
Heptane	1.387	410	1.30 (9%)	8.10 (91%)	7.50	0.13
		430	1.30 (11%)	8.10 (89%)	7.40	0.14
		455	1.20 (17%)	8.10 (83%)	6.90	0.15

The overlap integral, $J(\lambda)$, between the deconvoluted emission spectrum of the donor and the absorption spectrum of the acceptor AO, has been characterized for each emission peak and tabulated in Table V. Quenching of the fluorescence intensity of the donor in presence of the acceptor AO is shown in Fig. 5(c). The picosecond resolved FRET is clearly evident from Fig. 5(d), e, and f and Table IV.

As evident from Figs. 5, Table IV and Table V, the steady-state quenching and temporal behavior of the vibronic bands distinctly follows the individual overlap integral of the bands with the absorption of AO in the micelle.

The estimated D-A distance 2.48 nm is also found to be comparable to that of BP-Et distance.

TABLE III
COMPARISON OF THE FÖRSTER DISTANCE (R_0), OVERLAP INTEGRAL $J(\lambda)$ (BETWEEN DONOR BP EMISSION SPECTRUM AND ACCEPTOR ET ABSORPTION SPECTRUM) OBTAINED AT THE THREE DECONVOLUTED EMISSION PEAKS OF THE DONOR ALONG WITH THE ENERGY TRANSFER EFFICIENCY (E) AND DONOR-ACCEPTOR DISTANCE (R) CALCULATED FROM THE TIME RESOLVED EXPERIMENTS IN PRESENCE OF THE ACCEPTOR ET

Emission wavelength of donor BP (nm)	R_0 (nm)	$J(\lambda)$ (M^{-1} cm^{-1} nm^4)	E	r (nm)
410	2.16	1.09×10^{13}	64%	1.96
430	2.59	3.44×10^{13}	81%	2.03
455	2.47	1.12×10^{14}	84%	1.87

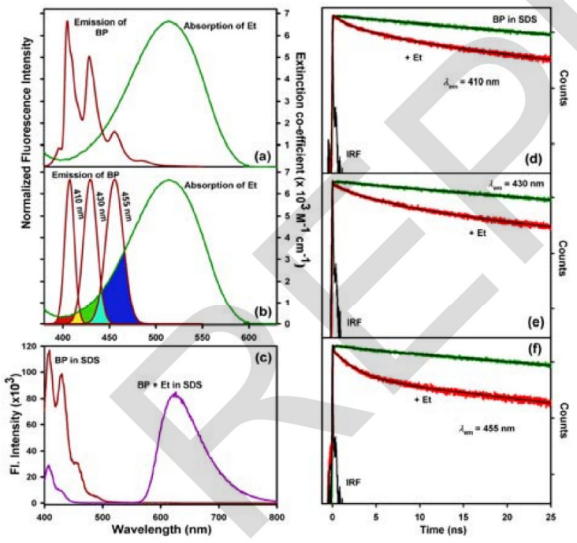

Figs. 4. Spectral overlap of BP emission and Et absorption in 100 mM SDS (~1.48 mM micellar concentration) without (a) and with (b) the deconvolution of the emission spectrum of BP at three specific wavelengths 410, 430 and 455 nm. (c) The emission spectrum of BP in SDS micelle before and after the addition of the acceptor Et. Picosecond resolved fluorescence transients of the donor BP molecules bound to SDS micelles with (red) and without (green) acceptor Et at (d) 410 nm, (e) 430 nm and (f) 455 nm. λ_{em} denotes emission wavelength. Excitation wavelength (λ_{ex}) is 350 nm for (a) and (b) and 375 nm for (c, d e and f). (Reprinted the colored/modified version of the original Figure in reference [50]with permission from reference [50]. Copyright 2013 WILEY-VCH Verlag GmbH & Co. KGaA, Weinheim)

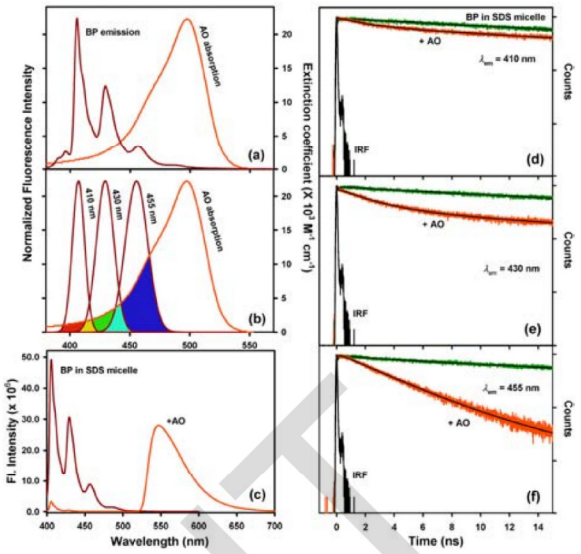

Figs. 5. Spectral overlap of BP emission and AO absorption in 100 mM SDS (~1.48 mM micellar concentration) without (a) and with (b) the deconvolution of the emission spectrum of BP at three specific wavelengths 410, 430 and 455 nm. (c) The emission spectrum of BP in SDS micelle before and after the addition of the acceptor AO. Picosecond resolved fluorescence transients of the donor BP molecules bound to SDS micelles with (orange) and without (green) acceptor AO at (d) 410 nm, (e) 430 nm and (f) 455 nm. λ_{em} denotes emission wavelength. Excitation wavelength (λ_{ex}) is 350 nm for (a) and (b) and 375 nm for (c, d e and f). (Reprinted the colored/modified version of the original Figure in reference [50]with permission from reference [50]. Copyright 2013 WILEY-VCH Verlag GmbH & Co. KGaA, Weinheim)

The energy acceptors Et and AO considered so far offer different degree of spectral overlap with all the vibronic bands of BP. The consequence of the differential $J(\lambda)$ with the vibronic bands are described in the earlier section.

Unambiguous evidence of the effect of differential $J(\lambda)$ with the vibronic bands on the corresponding FRET efficiency from the bands can be achieved in a control experiment, where the acceptor offers essentially no overlap with some bands and partial with others.

Use of crystal violet (CV) as potential acceptor offers essentially no overlap with band 1 (emission peak at 410 nm) and significant overlap with band 3 (emission peak at 455 nm). The interaction of CV probe molecules on SDS micelle has been investigated previously and concluded to reside at the surface of the micelle [48].

The overall and deconvoluted $J(\lambda)$s are shown in Figures 6(a) and (b), respectively. The overlap integral, $J(\lambda)$, between the deconvoluted emission spectrum of the donor and the absorption spectrum of the acceptor CV, has been characterized for each emission peak and tabulated in Table VI.

For the better view of the mentioned areas of overlap, between deconvoluted emission spectrum of the donor BP and absorption spectrum of acceptor CV, the overlapped region has been magnified and shown in Fig. 6(b) inset.

The steady-state fluorescence quenching of the donor BP in presence of the acceptor CV is shown in Fig. 6(c).

As evident from the Fig. 6(c), steady-state fluorescence quenching of BP occurs at all the vibronic bands of BP which can be due to formation of non-radiative donor-acceptor complexes in the ground state or due to energy transfer and hence steady-state fluorescence quenching is inconclusive as reported earlier [20], [37].

It has to be noted that band 3 is differentially quenched compared to others, as a consequence of larger $J(\lambda)$ with the acceptor CV.

To compare the energy transfer efficiency of the donor from its various vibronic structures, the fluorescence transients of the donor at its different emission peaks, 410, 430 and 455 nm have been monitored in absence and presence of the acceptor CV (Figs. 7 and Table IV).

The corresponding FRET parameters are tabulated in Table VI.

TABLE IV
THE LIFETIME COMPONENTS OF THE DONOR BP IN SDS MICELLE IN ABSENCE AND PRESENCE OF THE ACCEPTORS ET, AO AND CV. τ REPRESENTS THE TIME CONSTANTS IN NS AND THE NUMBERS IN THE PARENTHESIS REPRESENT RELATIVE CONTRIBUTION OF THE COMPONENT. τ_{Av} REPRESENTS THE AVERAGE LIFETIME IN NS. ERROR ±5%

Sample	Wavelength (nm)	τ_1 (ns)	τ_2 (ns)	τ_3 (ns)	τ_{av} (ns)
BP in SDS micelle	410	4.80 (3%)	30.70 (97%)		29.90
	430	2.90 (5%)	30.90 (95%)		29.50
	455	2.50 (10%)	30.70 (90%)		27.80
BP in SDS micelle + acceptor (Et)	410	0.50 (28%)	4.50 (36%)	25.40 (36%)	10.90
	430	0.10 (59%)	4.20 (23%)	24.90 (18%)	5.50
	455	0.10 (56%)	2.30 (30%)	27.00 (14%)	4.50
BP in SDS micelle + acceptor (AO)	410	0.10 (21%)	2.10 (24%)	28.20 (55%)	16.00
	430	0.10 (63%)	2.50 (22%)	25.20 (15%)	4.40
	455	3.50 (96%)	15.50 (4%)		4.00
BP in SDS micelle + acceptor (CV)	410	4.90 (3%)	30.70 (97%)		29.90
	430	0.10 (81%)	1.90 (3%)	24.80 (16%)	4.10
	455	0.10 (89%)	2.20 (1%)	24.70 (10%)	2.60

TABLE V
COMPARISON OF THE FÖRSTER DISTANCE (R_0), OVERLAP INTEGRAL $J(\lambda)$ (BETWEEN DONOR BP EMISSION SPECTRUM AND ACCEPTOR AO ABSORPTION SPECTRUM) OBTAINED AT THE THREE DECONVOLUTED EMISSION PEAKS OF THE DONOR ALONG WITH THE ENERGY TRANSFER EFFICIENCY (E) AND DONOR-ACCEPTOR DISTANCE (R) CALCULATED FROM THE TIME RESOLVED EXPERIMENTS IN PRESENCE OF THE ACCEPTOR AO

Emission wavelength of donor BP (nm)	R_0 (nm)	$J(\lambda)$ (M^{-1} cm^{-1} nm^4)	E	r (nm)
410	2.68	3.99×10^{13}	46%	2.75
430	3.08	9.59×10^{13}	85%	2.31
455	2.99	3.46×10^{14}	86%	2.21

TABLE VI
COMPARISON OF THE FÖRSTER DISTANCE (R_0), OVERLAP INTEGRAL $J(\lambda)$ (BETWEEN DONOR BP EMISSION SPECTRUM AND ACCEPTOR CV ABSORPTION SPECTRUM) OBTAINED AT THE THREE DECONVOLUTED EMISSION PEAKS OF THE DONOR ALONG WITH THE ENERGY TRANSFER EFFICIENCY (E) AND DONOR-ACCEPTOR DISTANCE (R) CALCULATED FROM THE TIME RESOLVED EXPERIMENTS IN PRESENCE OF THE ACCEPTOR CV

Emission wavelength of donor BP (nm)	R_0 (nm)	$J(\lambda)$ (M^{-1} cm^{-1} nm^4)	E	r (nm)
410	1.03	1.26×10^{11}	0%	-
430	1.32	6.04×10^{11}	86%	0.75
455	1.66	1.02×10^{13}	91%	1.13

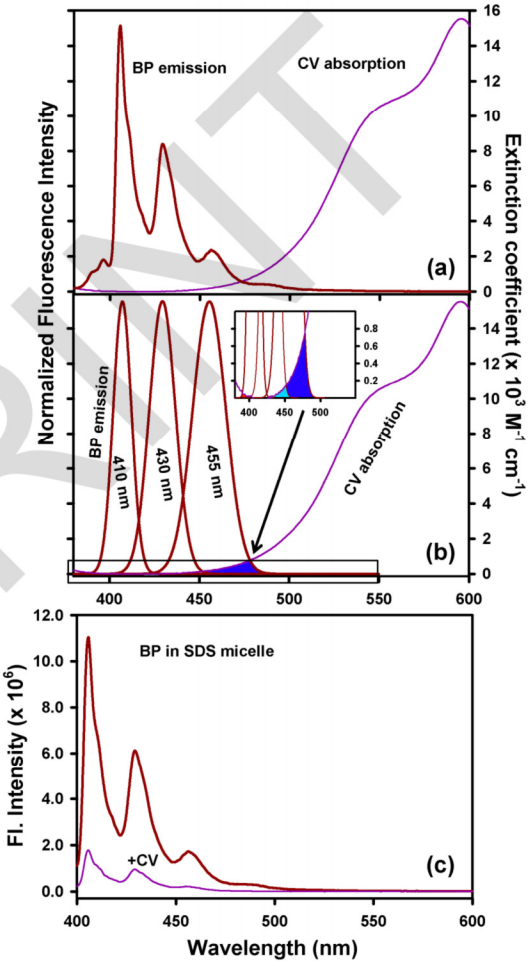

Figs. 6. Spectral overlap of BP emission and CV absorption in 100 mM SDS (~1.48 mM micellar concentration) without (a) and with (b) the deconvolution of the emission spectrum of BP at three specific wavelengths 410, 430 and 455 nm. Figure 6b inset is magnified view of the overlapped region marked by a rectangle on Figure 6b. (c) The emission spectrum of BP in SDS micelle before and after the addition of the acceptor CV [excitation wavelength (λ_{ex}) is 350 nm for (a) and (b) and 375 nm for (c)]. (Reprinted the colored/modified version of the original Figure in reference [50] with permission from reference [50]. Copyright 2013 WILEY-VCH Verlag GmbH & Co. KGaA, Weinheim)

As evident from the Fig. 6(b) inset, there is negligible or almost no overlap between the emission spectrum of BP at 410 nm and the CV absorption spectrum, which

consequently produces no fluorescence lifetime quenching of the donor BP at 410 nm in presence of the acceptor CV. However, there is significant lifetime quenching of the fluorophore at the other two vibronic bands (430 and 455 nm).

The observation is consistent with our previous results considering other two acceptors showing overlap integral dependent fluorescence lifetime quenching of the individual vibronic bands. Furthermore, the present observation, where we find no quenching at vibronic band 1 due to negligible overlap with the absorption of the acceptor CV, highlights the conclusive evidence of differential FRET from the vibronic bands of the donor BP.

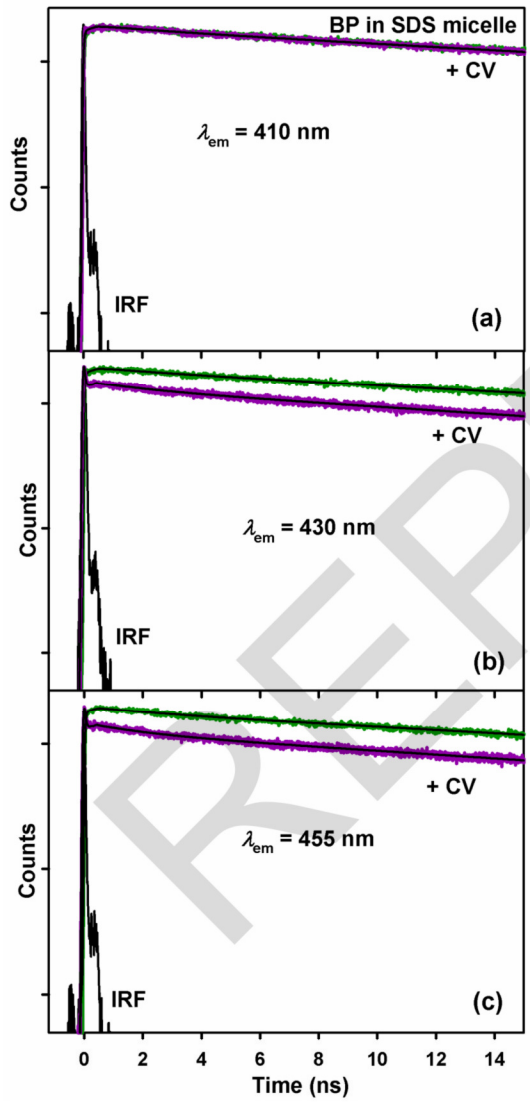

Figs. 7. Picosecond resolved fluorescence transients of the donor BP molecules bound to SDS micelles with (violet) and without (green) acceptor CV at (a) 410 nm, (b) 430 nm and (c) 455 nm. λ_{em} denotes emission wavelength. Excitation wavelength (λ_{ex}) = 375 nm. Reprinted the colored/modified version of the original Figure in reference [50] with permission from reference [50]. Copyright 2013 WILEY-VCH Verlag GmbH & Co. KGaA, Weinheim)

III.1.4. Comparison of the Differential Behaviour of the Vibronic Bands of BP under FRET with that of Different Dyes in a 'Dye Blend' Representing Different Electronic States

From our studies, the differential FRET from various vibronic bands of BP can be compared with the case of 'dye-blend' (mixture of dyes) under FRET to an energy acceptor in solution. In this regard, we have investigated FRET of a mixture of three quantum dots (QDs) having different emission maxima, to an energy acceptor CV. Figs. 8(a) and 8(b) respectively show the overall and deconvoluted spectral overlap between the emission spectra of the QDs (donor) and the absorption spectrum of the CV (acceptor) in toluene.

The overlap integral, $J(\lambda)$, between the deconvoluted emission spectrum of the donor QDs and the absorption spectrum of the acceptor CV, has been characterized and tabulated in Table VII. The picosecond resolved FRET is clearly evident from Figure 8(c) and Table VIII.

As evident from Figs. 8, Table VII and VIII, temporal behavior of the QDs in presence of the acceptor CV in toluene is comparable to the overlap integral dependent quenching behavior of the individual vibronic bands of BP with different acceptors in the micelle.

TABLE VII
COMPARISON OF THE FÖRSTER DISTANCE (R_0), OVERLAP INTEGRAL $J(\lambda)$ (BETWEEN DONOR QDS EMISSION SPECTRA AND ACCEPTOR CV ABSORPTION SPECTRUM) OBTAINED AT THE THREE DECONVOLUTED EMISSION PEAKS OF THE DONOR QDS ALONG WITH THE ENERGY TRANSFER EFFICIENCY (E) AND DONOR-ACCEPTOR DISTANCE (R) CALCULATED FROM THE TIME-RESOLVED EXPERIMENTS IN PRESENCE OF THE ACCEPTOR CV

Emission wavelength of donor QDs (nm)	R_0 (nm)	$J(\lambda)$ (M^{-1} cm^{-1} nm^4)	E	r (nm)
480	5.2	7×10^{15}	95%	3.2
570	6.0	16.7×10^{15}	97%	3.4
625	6.4	22.5×10^{15}	99%	2.9

TABLE VIII
THE LIFETIME COMPONENTS OF VARIOUS QDS AT THEIR CHARACTERISTIC EMISSION PEAKS IN ABSENCE AND PRESENCE OF ACCEPTOR CV. QDS MIXTURE CONSISTS OF QUANTUM DOTS QD480, QD570 AND QD625 HAVING EMISSION MAXIMA AT 480, 570 AND 625 NM, RESPECTIVELY. τ REPRESENTS THE TIME CONSTANT IN NS AND THE NUMBERS IN THE PARENTHESIS REPRESENT RELATIVE CONTRIBUTION OF THE COMPONENT. τ_{AV} REPRESENTS THE AVERAGE LIFETIME IN NS. ERROR ±5%

Sample	Emission Wavelength (nm)	τ_1 (ns)	τ_2 (ns)	τ_3 (ns)	τ_{av} (ns)
QDs mixture	480	0.80 (36%)	12.70 (64%)	-	8.40
	570	1.10 (25%)	11.40 (75%)	-	8.70
	625	1.10 (17%)	16.20 (83%)	-	13.60
QDs mixture +CV	480	0.10 (72%)	0.90 (24%)	4.40 (4%)	0.40
	570	0.10 (85%)	0.70 (13%)	4.80 (2%)	0.30
	625	0.10 (93%)	0.50 (6%)	3.00 (1%)	0.10

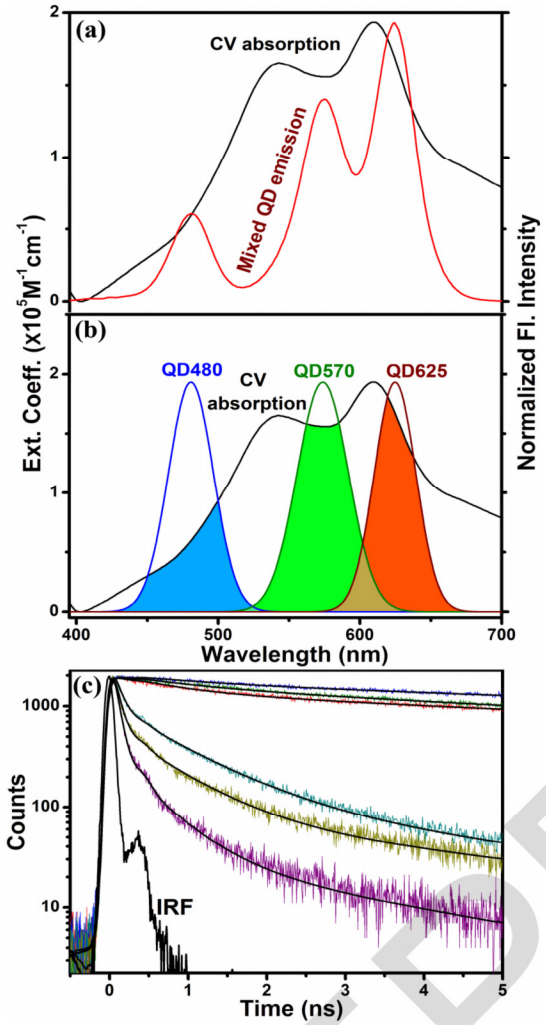

Figs. 8. Spectral overlap between the emission of mixed QDs (donor) and the extinction of CV (acceptor) without (a) and with (b) the deconvolution of the emission spectrum of mixed QDs at three specific wavelengths 480, 570 and 625 nm. (c) Picosecond resolved fluorescence transients of the donor (mixed QDs) monitored at 625 nm (blue), 570 nm (green) and 480 nm (red). The quenching of the fluorescence transients in presence of acceptor CV has been shown where cyan represents the decay transient of donor in presence of CV when monitored at 480 nm, yellow represents the decay transient of donor in presence of CV when monitored at 570 nm and magenta represents the decay transient of donor in presence of CV when monitored at 625 nm. Excitation wavelength (λ_{ex}) is 375 nm for all the cases. (Reprinted the colored/modified version of the original Figure in reference [50]with permission from reference [50]. Copyright 2013 WILEY-VCH Verlag GmbH & Co. KGaA, Weinheim)

III.1.5. Verification of the Introduced Method of Differential FRET Calculation Employing the Standard Theoretical Framework and D-A Distribution

The suitability of the differential over integral analysis procedure introduced in the present study in the standard theoretical frame work for the FRET to estimate average number of quenchers/quenching constants developed by Infelta and Tachiya [39] has also been investigated.

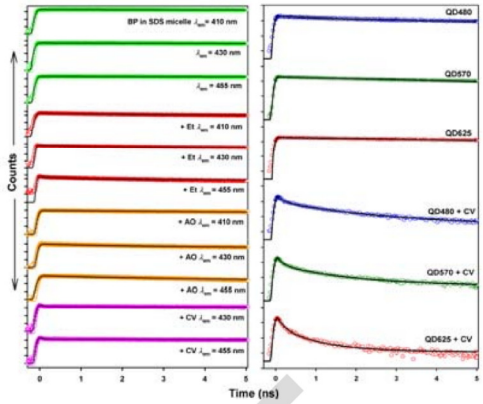

Fig. 9. Left panel shows the fluorescence transients of the donor BP molecules bound to SDS micelle with (red, orange and pink circles) and without (green circles) acceptors Et, AO and CV molecules monitored at different wavelengths 410, 430 and 455 nm. Red, orange and pink colours in the fluorescence transients of BP represent the presence of Et, AO and CV acceptors in the micelle respectively. Right panel shows the fluorescence transients of the donor QDs (a) QD480 (blue) (b) QD570 (dark green) and (c) QD625 (dark red) in toluene in absence and presence of the acceptor CV. All the transients are fitted with the kinetic model developed by Infelta and Tachiya (see text). The Y-axis (Normalized Fl. Intensity) is presented in log scale and the baselines of the transients are vertically shifted for clarity. (Reprinted the colored/modified version of the original Figure in reference [50]with permission from reference [50]. Copyright 2013 WILEY-VCH Verlag GmbH & Co. KGaA, Weinheim)

We have determined the values of the parameters m, k_q, and k_0 as described under materials and methods section by fitting the Eq. (12) to the decay curves of the donor BP molecules in the absence and presence the acceptors Et, AO and CV (Fig. 9 left panel and Table IX). Fig. 9 left panel shows the time resolved fluorescence transients of BP monitored at its different emission peaks, 410, 430 and 455 nm in absence and presence of Et, AO and CV fitted with Eq. (12). Since our time resolved studies (Figs. 7(a) and Table IV) show that CV does not quench the fluorescence lifetime of the donor BP at 410 nm, the corresponding fluorescence transient has not been fitted with the equation of the kinetic model (Eq. (12)). As evident from the Fig. 9 left panel, the model describes the decay curves reasonably well. The quenching parameters are summarized in Table IX. Upon fitting the decay curves of BP with the kinetic model mentioned before, it is apparent that the distribution of acceptor molecules on the micellar surface does not change with the wavelength at which the donor emission is monitored. As summarized in Table IX, the mean number of acceptor molecules associated with the micelle (m) remains same as 0.8, 1 and 0.7 respectively for Et, AO and CV at the three wavelengths corresponding to the three emission peaks of BP. The value of 'm' being independent of the vibronic structure of the donor provides authenticity of the analysis procedure. However, the value of quenching rate constant (k_q) due to the acceptors depends on the wavelength at which the donor emission is monitored, being maximum at 455 nm and minimum at 410 nm with an intermediate value at 430 nm.

TABLE IX
VALUES OF THE QUENCHING PARAMETERS USING THE SIMPLIFIED VERSION OF THE KINETIC MODEL BY INFELTA AND TACHIYA

Sample	λ_{em} (nm)	K_0 (ns^{-1})	K_q (ns^{-1})	m
BP in SDS micelle	410	0.032	-	-
	430	0.032	-	-
	455	0.032	-	-
BP + Et in SDS micelle	410	0.032	0.24	0.8
	430	0.032	0.35	0.8
	455	0.032	0.64	0.8
BP + AO in SDS micelle	410	0.032	0.07	1
	430	0.032	0.27	1
	455	0.032	0.30	1
BP + CV in SDS micelle	430	0.032	8.97	0.7
	455	0.032	9.23	0.7

The nature of change in k_q being similar to that of energy transfer efficiency mentioned before, holds well to the fact that k_q is also proportional to the overlap integral between the donor emission and acceptor absorption. Further studies are required for the better understanding of the observed variation of k_q with the emission wavelength of the donor BP molecules. The total decay constant (k_0) of the excited probe in absence of a quencher, remains same at all the three monitored wavelengths with a value of 0.032 ns^{-1}.

The above mentioned kinetic model has also been applied for the quenching of QDs by the acceptor CV in toluene. We have determined the values of the parameters m_t, k_{qt}, k_0, m, and k_q by fitting equations (13) and (14) to the decay curves of QDs in the absence and presence of acceptor (as described in materials and methods section) and tabulated in Table X. The corresponding fitting curves are shown in Figure 9 right panel. In order to get idea of the probability distribution of donor-acceptor distance, we have analyzed the time resolved decay transients of donor BP in presence and absence of acceptor Et, as shown in Figure 10(a) to construct the distance distribution function, P(r) (see experimental section for details). As evident in Figures 10(b), (c) and (d), the half width (hw) of the distance distribution is found to be 3.3 Å for all the three vibronic bands under consideration. Similarly, for QDs the fluorescence transients of donor QD480, QD570 and QD625 in toluene in absence and presence of the acceptor CV have been fitted upon considering the distance distribution between donor and acceptor in toluene as shown in Fig. 11(a) and the hw of the distance distribution has been found to be 3.3, 4.4 and 3.3 Å for QD480, QD570 and QD625, respectively as shown in Figs. 11(b), (c) and (d).

III.2. UVA Radiation Induced Ultrafast Electron Transfer from a Food Carcinogen Benzo[a]pyrene to Organic Molecules, Biological Macromolecules and Inorganic Nano Structures

In this section, we have discussed the use of a well known electron acceptor [57], para-benzoquinone (BQ) as an organic molecule to emphasize the electron donating efficiency of BP upon excitation with UVA radiation, using a laser source of 375 nm. Both DNA and protein have been used as biological macromolecules to monitor the ET from BP in presence of UVA radiation. In addition, we have used zinc oxide (ZnO) nanorods (NRs)-based photodevice to directly monitor such photo-induced ET reaction from BP to the NRs. In order to study ET reaction from BP to organic molecules and macromolecules along with inorganic NRs, we have used both steady-state and picosecond-resolved fluorescence spectroscopy. Structural perturbation of DNA in the presence of BP has been investigated through temperature-dependent circular dichroism (CD) spectroscopy. Furthermore, to monitor the effect of temperature on ET from BP to biological macromolecules, we have discussed temperature-dependent steady-state and time-resolved fluorescence spectroscopic studies [21].

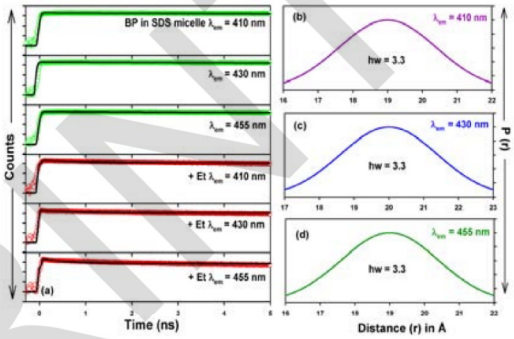

Figs. 10. (a) Fluorescence transients of BP in SDS micelle in absence and presence of the acceptor Et, monitored at 410, 430 and 455 nm and fitted upon considering the distance distribution between donor and acceptor in SDS micelle. The probability of distance distribution (P(r)) with respect to mean distance between donor BP and acceptor Et for different vibronic bands under consideration having emission maxima at (b) 410, (c) 430 and (d) 455 nm. (Reprinted the colored/modified version of the original Figure in reference [50] with permission from reference [50]. Copyright 2013 WILEY-VCH Verlag GmbH & Co. KGaA, Weinheim)

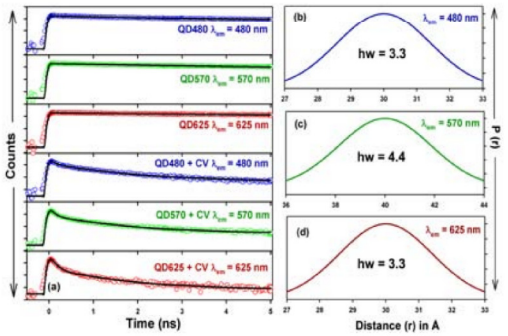

Figs. 11. (a) Fluorescence transients of QD480, QD570 and QD625 in toluene in absence and presence of the acceptor CV and fitted upon considering the distance distribution between donor and acceptor in toluene. The probability of distance distribution (P(r)) with respect to mean distance between the donor QDs (b) QD480 (c) QD570 and (d) QD625 and acceptor CV in toluene. (Reprinted the colored/modified version of the original Figure in reference [50] with permission from reference [50]. Copyright 2013 WILEY-VCH Verlag GmbH & Co. KGaA, Weinheim)

TABLE X
OVERVIEW OF THE VALUE OF QUENCHING PARAMETERS FOR QUANTUM DOTS IN ABSENCE AND PRESENCE OF ACCEPTOR CV USING KINETIC MODEL DEVELOPED BY INFELTA AND TACHIYA. λ_{EM} REPRESENTS EMISSION WAVELENGTH

Sample	λ_{em} (nm)	k_o[ns^{-1}]	m_t	k_{qt}[ns^{-1}]	m	k_q[ns^{-1}]
QDs mixture	480	0.07	0.41	0.67	-	-
	570	0.095	0.21	0.50		
	625	0.03	1.12	0.06		
QDs mixture + CV	480	0.07	3.31	0.38	0.93	6.40
	570	0.095	2.86	0.62	1.43	8.46

III.2.1. Electron Transfer Reaction from BP to BQ

Fig. 12(a) shows the steady-state fluorescence quenching of benzo[*a*]pyrene (BP) in DMSO with increasing concentration of para-benzoquinone (BQ), which is a well-known electron acceptor [57]-[58].

The fluorescence spectrum of BP in absence of the quencher strongly corroborates with the spectral nature of BP emission reported earlier in different solvents [6].

While BP monomers produce three well characterized emission peaks around 410, 430 and 455 nm and a weak band near 485 nm due to different vibrational bands, BP aggregates are known to produce an emission feature that peaks around 490 nm [6].

Since a very low concentration of BP (1 μM) has been used in our sample, the contribution of aggregates does not appear to be significative.

The observed decrease in fluorescence intensity of BP in the presence of BQ can arise either due to collisional/dynamic or static quenching or both or even through non-molecular mechanisms where fluorophore itself or other absorbing species attenuates the incident light [37].

For a better insight on the mechanism of the observed quenching, the relative change in fluorescence intensity of BP has been plotted as a function of the quencher (BQ) concentration at the different vibronic peaks of 410, 430 and 455 nm as shown in Figs. 12(b), (c) and (d), respectively.

For collisional quenching the decrease in fluorescence intensity is described by the well-known Stern-Volmer (SV) equation [37]:

$$\frac{F_0}{F} = 1 + k_q \tau_0 [Q] = 1 + K_{SV} [Q] \qquad (19)$$

F_0 and F are the fluorescence intensities in the absence and presence of quencher, respectively; k_q is the bimolecular quenching constant; τ_0 is the lifetime of the fluorophore in the absence of quencher, and $[Q]$ is the concentration of quencher.

The Stern-Volmer quenching constant is given by $K_{SV} = k_q \tau_0$. In case of dynamic quenching, the SV plot (F_0/F vs $[Q]$) becomes linear with an intercept of one on the y-axis and a slope equivalent to the dynamic quenching constant (K_D) [37].

However, as evident from Figs. 12(b), (c), and (d), the SV plots for the fluorescence quenching of BP by BQ (monitored at different wavelengths) appear as an upward curvature, concave towards the y-axis.

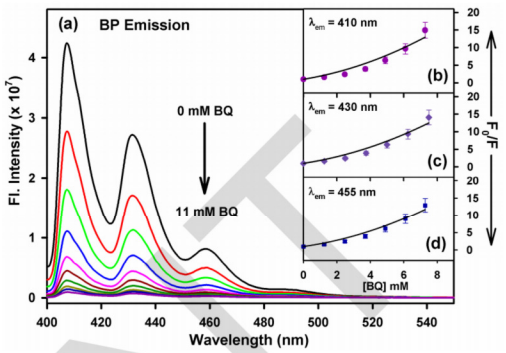

Figs. 12. (a) Fluorescence quenching spectra of 1μM benzo[*a*]pyrene (BP) in DMSO with increasing concentrations of benzoquinone (BQ) (0, 1.25, 2.50, 3.75, 5.0, 6.25, 7.5, 8.75, 10 and 11 mM). Plots of F_0/F vs. BQ concentration at 410 nm (b), 430 nm (c) and 455 nm (d). F_0 and F represent fluorescence intensity of the fluorophore (BP) in absence and presence of the quencher (BQ), respectively. Excitation wavelength (λ_{ex}= 375 nm). (Reprinted with permission from reference [21]. Copyright 2013, American Chemical Society)

Such curved SV plots are typical for fluorophores which are quenched simultaneously by collisions (dynamic quenching) and non-fluorescent ground state complex formation (static quenching) with the same quencher [37].

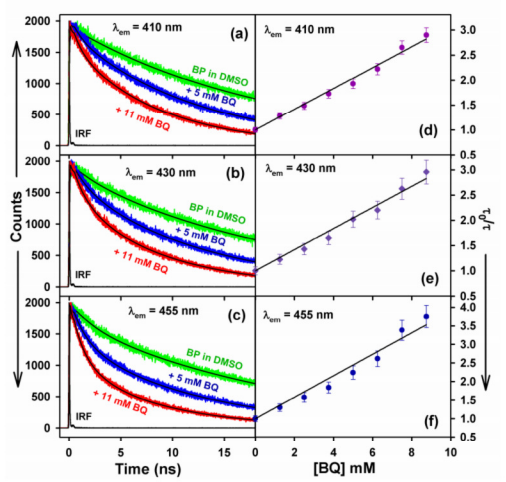

Figs. 13. Picosecond-resolved fluorescence transients of BP in DMSO in absence and presence of different BQ concentrations and the corresponding plots of τ_0/τ vs. BQ concentration monitored at (λ_{em}) 410 nm (a and d), 430 nm (b and e) and 455 nm (c and f). τ_0 and τ represent lifetimes of the fluorophore (BP) in absence and presence of the quencher (BQ), respectively. Excitation wavelength (λ_{ex}= 375 nm). (Reprinted with permission from reference [21]. Copyright 2013, American Chemical Society)

When both static and dynamic quenching occur for the same fluorophore, the SV equation gets modified as [37]:

$$\frac{F_0}{F} = \left(1 + K_D[Q]\right)\left(1 + K_S[Q]\right) \quad (20)$$

where K_S represents the static quenching constant. The modified form of the SV equation being second order in [Q], accounts for the upward curvature in our SV plots shown in Figures 12(b), (c) and (d).

The dynamic portion of the observed quenching has been determined by lifetime measurements. Fluorescence transients of BP in the absence and presence of different concentrations of BQ monitored at 410, 430 and 455 nm are presented in Figs. 13(a), (b) and (c), respectively.

The lifetime components of the transients are tabulated in Table XI. As evident from Table XI, a fast component of 2 ns appears in the fluorescence transients of BP at emission wavelengths of 430 and 455 nm both in the absence and presence of the quencher, which accounts for the presence of some BP aggregates in the experimental solution, having higher contribution at 455 nm compared to that at 430 nm, while at 410 nm the fluorescence originates essentially from the BP monomers.

Furthermore, it has also been observed that the contribution of the 2 ns component in the fluorescence transient of BP enhances with the increase in BP concentration due to the progressive formation of BP aggregates. As BP monomers are known to produce a weak band near 485 nm[6], at 490 nm both the emission from BP monomers and BP aggregates have significant contribution. However, as expected, the 2 ns component (due to BP aggregates) found to have higher contribution (27%) in the fluorescence transient of BP at 490nm compared to that at 430 (7%) or 455 nm (15%).

The relative contribution of 2 ns component in the fluorescence transients of BP further increases at 520 (31%) and 560 nm (33%), due to the relatively higher contribution of BP aggregates (data not shown). For dynamic quenching, the average lifetimes in the absence (τ_0) and presence (τ) of quencher are given by [37]:

$$\frac{\tau_0}{\tau} = 1 + k_q \tau_0 [Q] = 1 + K_D[Q] \quad (21)$$

The numerical values of τ_0 and τ at three different wavelengths are given in Table XI. τ_0 values are obtained as 19.32, 18.75 and 17.53 ns at 410, 430 and 455 nm, respectively. Plots of τ_0/τ vs quencher concentrations for the lifetime quenching of BP with increasing concentrations of BQ, yield a straight line with an intercept of one as shown in Figures 13(d), (e) and (f) for emission wavelengths (λ_{em}) 410, 430 and 455 nm, respectively.

The K_D values are obtained as 0.21 ± 0.01, 0.21 ±0.01 and 0.29 ±0.02 mM^{-1} and the corresponding values of k_q are 10.87×10^9, 11.20×10^9 and 16.54×10^9 M^{-1} s^{-1} while monitoring lifetime quenching at 410, 430 and 455 nm, respectively.

The k_q values obtained for BP are comparable to that of hypericin fluorescence quenching by the same quencher BQ, reported previously [59]. As shown in Figs. 12(b), (c) and (d), upon fitting the plots of F_0/F vs [Q] with Eq. (20) considering the K_D values obtained from time-resolved studies, the values of K_S obtained at 410, 430 and 455 nm are 0.57±0.08, 0.51±0.08 and 0.38±0.06 mM^{-1}, respectively.

The quenching in lifetime being a measure of the rate process that depopulates the excited state can arise either due to energy transfer or electron transfer (ET) reactions.

Since there is no overlap between the emission spectrum of BP and the absorption spectrum of BQ, the possibility of energy transfer from BP to BQ can be neglected, attributing the quenching to ET reactions.

As evident from Table XI, at low quencher concentrations (1.25, 2.50 and 3.75 mM) the fluorescence transients of BP exhibit an ultrafast component around 500 ps while at higher BQ concentrations (5 to 11 mM) the fluorescence transients of the same exhibit two ultrafast components (~100 and ~ 800 ps) comparable to the ET components reported earlier in porphyrin-BQ models separated by different distances [60]. Such multiple ET components in the fluorescence transients of BP at different BQ concentrations strongly corroborate with the non-exponential nature of ET reactions and those components are attributed to the various modes of association (side to side or face to face) along with the different distances between BP and BQ in the solvent which control the ET rates[60].

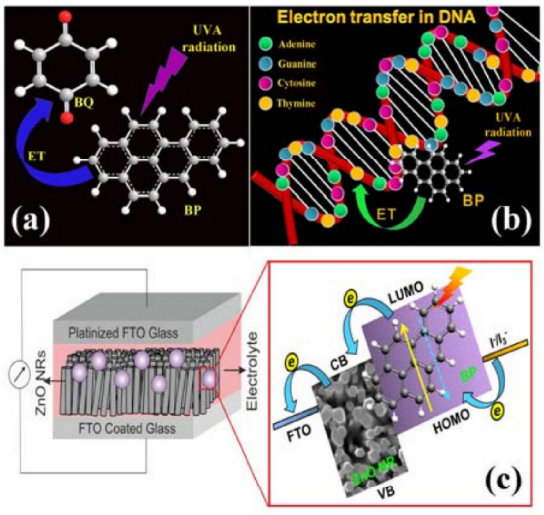

Scheme 1. UVA radiation induced electron transfer (ET) from benzo[*a*]pyrene (BP) to (a) organic molecule, benzoquinone (BQ) and (b) biological macromolecule, DNA. (c) Schematic representation of a model ZnO NR (gray)-based photodevice. BP (purple) molecules are anchored on ZnO NRs by surface adsorption. The charge separation and interparticle charge migration processes of the entire photodevice structure are shown. (Reprinted with permission from reference [21]. Copyright 2013, American Chemical Society

TABLE XI
THE LIFETIME COMPONENTS OF BP, AT ITS CHARACTERISTICS EMISSION PEAKS IN PRESENCE OF DIFFERENT QUENCHER (BQ) CONCENTRATIONS ([*Q*]). λ_{EM} REPRESENTS THE EMISSION WAVELENGTH. τ REPRESENTS THE TIME CONSTANT IN NS AND THE NUMBERS IN PARENTHESIS REPRESENT RELATIVE CONTRIBUTION OF THE COMPONENT. τ_{Av} REPRESENTS THE AVERAGE LIFETIME IN NS AND IS EQUIVALENT TO τ_0 AT [Q] = 0. $\tau_{Av} = \tau$ AT [Q] ≠ 0. ERROR ±5%

[Q] mM	λ_{em} (nm)	τ_1 (ns)	τ_2 (ns)	τ_3 (ns)	τ_4 (ns)	τ_{av} (ns)	τ_0/τ
0.00	410	19.32 (100%)				19.32	1.00
	430	2.00 (7%)	20.01 (93%)			18.75	1.00
	455	2.00 (15%)	20.27 (85%)			17.53	1.00
1.25	410	0.50 (10%)	16.67 (90%)			15.05	1.28
	430	0.50 (4%)	2.00 (9%)	17.32 (87%)		15.27	1.23
	455	0.50 (8%)	2.00 (16%)	17.24 (76%)		13.46	1.30
2.50	410	0.5 (12%)	14.72 (88%)			13.01	1.49
	430	0.50 (6%)	2.00 (10%)	15.34 (84%)		13.12	1.43
	455	0.50 (12%)	2.00 (18%)	15.33 (70%)		11.15	1.57
3.75	410	0.5 (16%)	13.22 (84%)			11.19	1.73
	430	0.50 (6%)	2.00 (14%)	13.83 (80%)		11.37	1.65
	455	0.50 (14%)	2.00 (20%)	13.76 (66%)		9.55	1.84
5.00	410	0.10 (4%)	0.80 (14%)	12.06 (82%)		10.01	1.93
	430	0.10 (8%)	0.80 (8%)	2.00 (12%)	12.46 (72%)	9.28	2.02
	455	0.10 (9%)	0.80 (13%)	2.00 (19%)	12.42 (59%)	7.82	2.24
6.25	410	0.10 (8%)	0.80 (15%)	11.13 (77%)		8.70	2.22
	430	0.10 (8%)	0.80 (8%)	2.00 (13%)	11.52 (71%)	8.51	2.20
	455	0.10 (11%)	0.80 (15%)	2.00 (20%)	11.42 (54%)	6.70	2.62
7.50	410	0.05 (14%)	0.80 (16%)	10.22 (70%)		7.29	2.65
	430	0.05 (14%)	0.80 (9%)	2.00 (13%)	10.62 (64%)	7.14	2.63
	455	0.05 (21%)	0.80 (18%)	2.00 (16%)	10.46 (45%)	5.18	3.38
8.75	410	0.05 (15%)	0.90 (17%)	9.57 (68%)		6.67	2.90
	430	0.05 (15%)	0.80 (12%)	2.00 (12%)	9.83 (61%)	6.34	2.96
	455	0.05 (21%)	0.80 (20%)	2.00 (16%)	9.72 (43%)	4.67	3.75
10.0	410	0.04 (20%)	0.80 (17%)	8.84 (63%)		5.71	3.38
	430	0.04 (21%)	0.80 (11%)	2.00 (13%)	9.23 (55%)	5.43	3.45
	455	0.04 (26%)	0.80 (20%)	2.00 (18%)	9.20 (36%)	3.84	4.57
11.0	410	0.04 (21%)	0.80 (18%)	8.34 (61%)		5.24	3.69
	430	0.04 (18%)	0.80 (15%)	2.00 (13%)	8.68 (54%)	5.07	3.70
	455	0.04 (28%)	0.80 (21%)	2.00 (18%)	8.61 (33%)	3.38	5.19

As evident from earlier studies [58], BQ has a positive electron affinity of 1.89 eV and forms a stable negative ion through charge transfer collisions. Furthermore, pyrene class of molecules are known to have a lower electron affinity (0.59 eV) [61] compared to BQ that further supports the ET from BP to BQ leading to the observed quenching in the fluorescence lifetime of BP with increasing BQ concentrations.

III.2.2. Ultrafast Charge Transfer Reactions Between BP and Biological Macromolecules

Upon monitoring the ET reaction from BP to BQ molecule as shown in Scheme 1(a), another macromolecule, calf-thymus DNA (CT-DNA), has been considered to investigate the mode of interaction between BP and CT-DNA upon exciting the former with UVA radiation (Scheme 1(b)). It has to be noted, as CT-DNA absorbs weakly above 300 nm [62], it will have negligible effect on the emission property of BP upon exciting the solution of BP-CT-DNA complex at 375 nm.

Fig. 14(a) shows the temperature-dependent fluorescence spectra of BP-CT DNA complex. Emission spectra of BP in the presence of CT-DNA, show that the relative emission intensities of BP at the resolved peaks (410, 430 and 455 nm) are much higher compared to that of the aggregate peak around 490 nm. The relatively lower emission intensity of the aggregate peak compared to that of the monomer BP peaks in presence of CT-DNA is clear evidence of association between the two, particularly at low temperatures where the solubility of BP in aqueous medium is negligible being at around 10^{-8} M. As shown in the Fig. 14(a), the emission intensities of BP in CT-DNA enhance with the increase in temperature.

Fig. 14(a) inset shows the emission intensities of the same, monitored at 410 nm as a function of temperature, where the enhancement in the emission intensity appears to initiate at about 25°C. To selectively monitor the interaction between BP monomers and the CT-DNA, fluorescence transients have been monitored at 410 nm where the contribution of BP aggregates is minimum or negligible.

Fig. 14(b) shows the picosecond-resolved fluorescence transients of BP-CT-DNA complex at 20 and 87°C. The purpose of choosing high temperature around 87°C was to attain the melting temperature of genomic DNA, which has earlier been reported [63] to be 83°C.

The corresponding lifetime components of the complex have been tabulated in Table XII. The ultrafast time components of 50 and 900 ps being comparable with the ET components observed in the fluorescence transient of BP undergoing ET reaction with BQ, are attributed to the UVA radiation induced ET between BP and DNA.

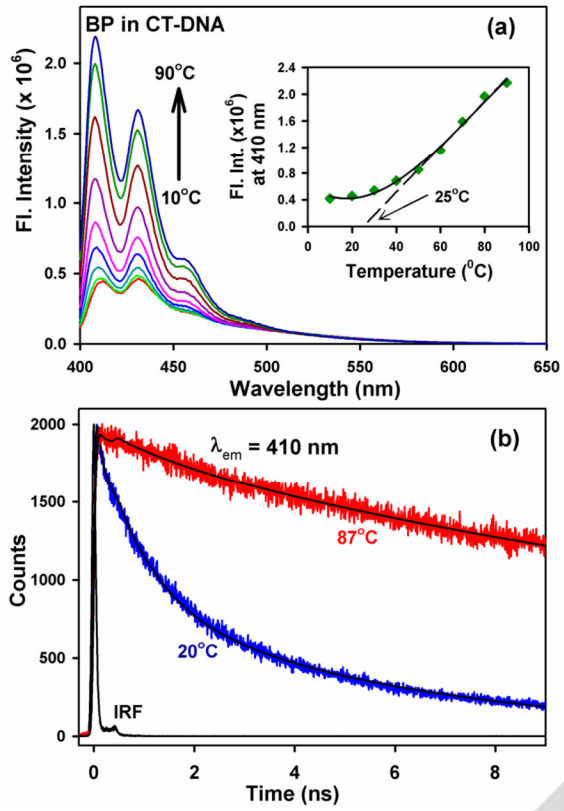

Figs. 14. (a) Fluorescence spectra of BP in CT-DNA at different temperatures. Inset shows the fluorescence intensity of the same at 410 nm as a function of temperature and the bold line is the cubic polynomial fit. The broken line is the extrapolated linear fit of the exponentially rising part of the plot, where the intercept at x-axis represents the initiation temperature for such rise in the fluorescence intensity. (b) Picosecond-resolved fluorescence transients of the same at 20° and 87°C. Excitation wavelength (λ_{ex}= 375 nm). (Reprinted with permission from reference [21]. Copyright 2013, American Chemical Society)

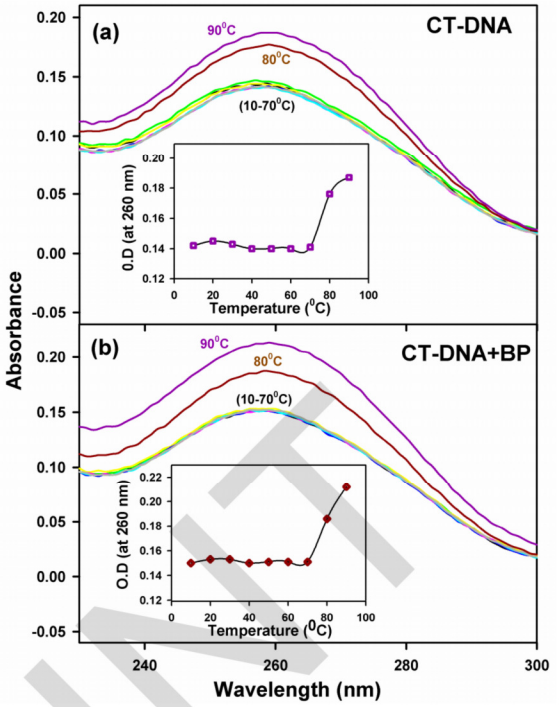

Figs. 15. Temperature dependent absorption spectra of CT-DNA as a function of wavelength in absence (a) and presence (b) of BP. Insets show the respective optical density (O.D) at 260 nm with increase in temperature where solid lines are the guide to the eye. (Reprinted with permission from reference [21]. Copyright 2013, American Chemical Society)

Ionisation potential of aromatic hydrocarbons being lower than the nitrogenous bases in DNA [26] and pyrimidines being better electron acceptors than purines, it can be concluded that in the ET complex between BP and CT-DNA, electron flows from BP to DNA through the pyrimidine bases.

As evident from Figure 14(b) and Table XII, the relative contribution of the ET components of 50 and 900 ps decreases from 40 to 4% and from 33 to 11%, respectively, with the increase in temperature from 20 to 87°C. The time-resolved studies strongly corroborate with the temperature-dependent steady-state emission results of BP in CT-DNA as shown in Figure 14(a), endorsing the fact that with the melting of DNA, the ET pathway from BP to DNA gets interrupted resulting in the enhancement of emission intensity of BP along with its excited state lifetime.

The interruption in ET pathway from BP to DNA with the DNA melting can arise either due to the release of BP from DNA or due to the binding of BP to single stranded DNA in an orientation unfavourable for ET.

As evident from Fig. 14(b) and Table XII, the fluorescence transient of BP in CT-DNA at 87°C can be fitted triexponentially with time components of 100 ps (4%), 800 ps (11%) and 22.04 ns (85%) while BP in buffer at 87°C produces a single lifetime component of 23 ns. Therefore, upon comparing the lifetime of BP in CT-DNA with that in buffer at 87°C, it can be concluded that at such high temperature, 85% of the DNA bound BP molecules get released to the surrounding buffer.

The observed perturbation of ET from BP to CT-DNA, with the increase in temperature, motivated us to investigate the structural change of the latter associated with such thermal enhancement. Figures 15a and b show the absorption spectra of CT-DNA at different temperatures in absence and presence of BP, respectively. As evident from the Figures 15(a) and (b), the absorption spectra of CT-DNA do not show any significant change while enhancing the temperature upto 70^0C. The corresponding melting curves of CT-DNA, constructed from the absorbance at 260 nm[64] while increasing the temperature upto 90^0C are shown in the insets of Figs. 15(a) and (b) respectively.

As evident from the insets of Figs. 15(a) and (b), both the curves look alike and do not reach the saturation at 90^0C (upto which the temperature was enhanced) which suggest that BP induced structural changes in CT-DNA cannot be manifested through temperature dependent absorption spectroscopy.

TABLE XII
FLUORESCENCE LIFETIME COMPONENTS (τ) OF BP IN BUFFER AND UPON INTERACTION WITH CT-DNA AT DIFFERENT TEMPERATURES ALONG WITH THE ROTATIONAL TIME CONSTANTS (τ_R). EMISSION WAVELENGTH (λ_{EM}) AND EXCITATION WAVELENGTH (λ_{EX}) ARE 410 AND 375 NM RESPECTIVELY. THE NUMBERS IN PARENTHESIS REPRESENT RELATIVE CONTRIBUTION OF THE COMPONENT. τ_{AV} REPRESENTS THE AVERAGE LIFETIME IN NS. ERROR ±5%

Sample	Temperature (°C)	τ_1 (ns)	τ_2 (ns)	τ_3 (ns)	τ_{av} (ns)	Anisotropy	
						τ_r (ns)	Offset
BP in CT-	20	0.05 (40%)	0.90 (33%)	5.61 (27%)	1.52	0.14	0.15
DNA	87	0.10 (4%)	0.80 (11%)	22.04 (85%)	18.83	0.07	0.01
BP in buffer	87	23.08 (100%)			23.08	0.05	0.00

Hence we have used the temperature dependent CD spectroscopy to monitor the BP induced structural changes in the CT-DNA. Insets of Figs. 16(a) and (b) show the temperature-dependent optical rotation of CT-DNA in the absence and presence of BP, respectively. As evident from the insets of Figs. 16(a) and (b), at low temperatures, a positive peak around 270 nm and a negative peak around 245 nm in the far UV spectrum are in accordance with the average secondary structure of DNA [63] and the corresponding UV absorption spectra are dominated by the DNA absorption as shown in the Figs. 15(a) and (b).

Therefore, it is difficult to infer the structural perturbation of CT-DNA in the presence of BP at low temperatures.

It is clear from the insets of Figures 16(a) and (b) that the peak at 270 nm is mostly affected by the temperature induced melting of the DNA. The change in the optical rotation associated with this peak has been monitored to construct the temperature-induced melting of the CT-DNA in the absence and presence of BP, as shown in Figs. 16(a) and (b), respectively.

As evident from the Figures, the corresponding DNA melting curves do not reach the saturation level at 90°C, up to which the temperature of the DNA has been raised. Thus, melting temperatures of CT-DNA in the absence and presence of BP cannot be calculated from the respective melting curves following the standard procedures. However, the temperature at which the melting initiates for either case can be approximated, by extrapolating the exponential part of the melting curves on x-axis.

Though the temperatures are deduced from only three data points in each case, the overall nature of the temperature dependent change in the optical rotation of CT-DNA at 270 nm is completely different in absence and presence of BP, as shown in Figs. 16(a) and (b). The uncertainties in the temperature, at which the DNA melting initiates, being same for both the cases (in absence and presence of BP), have not been considered.

The corresponding temperatures, at which DNA melting initiates in the absence and presence of BP, have been found out to be 65 and 59°C respectively.

The initiation of DNA melting at comparatively lower temperature in the presence of BP is a clear signature of the association of BP with DNA, leading to the weakening of hydrogen bonds between the two DNA strands. Thus, lower thermal energy is required to initiate DNA melting in the presence of BP compared to that in its absence.

Here, it has to be noted that the initiation temperature observed for the enhancement in emission intensity of BP in CT-DNA (Fig. 14(a) inset) is much lower compared to that of BP assisted DNA melting, which signifies that perturbation in ET from BP to CT-DNA initiates at some lower temperature prior to the DNA melting. Such perturbation in ET before the onset of DNA melting can arise due to some changes in the orientation of DNA bound BP molecules, interfering in the ET pathway.

For better understanding of the fate of BP with the melting of DNA, the fluorescence anisotropies of BP have been monitored in the presence of DNA at 20°C and at DNA melting temperature (~87°C), as shown in Figs. 17(a) and (b), respectively.

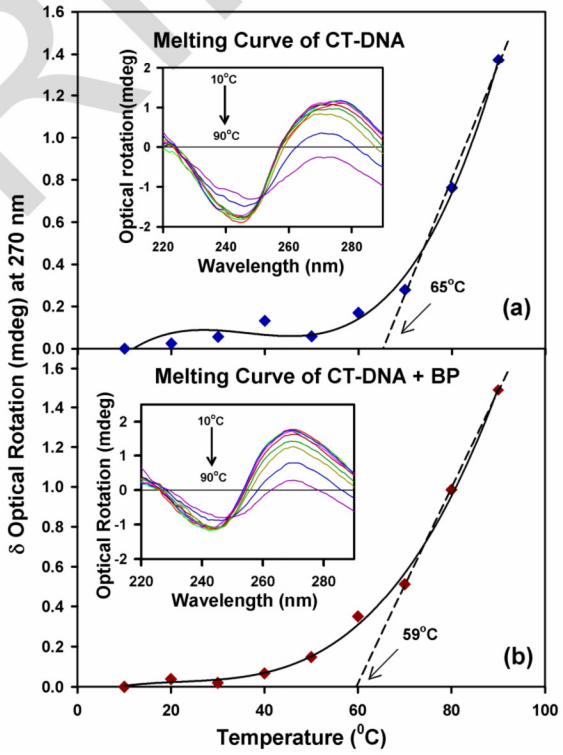

Figs. 16. Difference in optical rotation (mdeg) of CT-DNA at 270 nm with increase in temperature in absence (a) and presence (b) of BP. Insets show the respective temperature-dependent optical rotation of the CT-DNA as a function of wavelength. Solid lines are the cubic polynomial fit. The broken lines are the extrapolated linear fits where the intercepts at x-axis represent the initiation temperature of the corresponding melting processes. (Reprinted with permission from reference [21]. Copyright 2013, American Chemical Society)

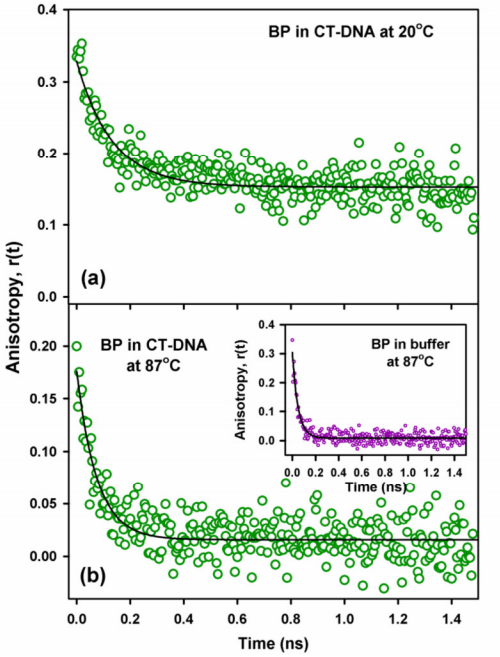

Figs. 17. Fluorescence anisotropy of BP in CT-DNA at (a) 20°C and (b) 87°C and in 50 mM phosphate buffer at 87°C (inset of b). Solid lines indicate exponential fitting of the experimental data points. (Reprinted with permission from reference [21]. Copyright 2013, American Chemical Society)

The rotational time constants (τ_r) of BP in DNA have been calculated from the respective fluorescence anisotropies and have been compared with that of BP in phosphate buffer at 87°C (inset of Fig. 17(b)).

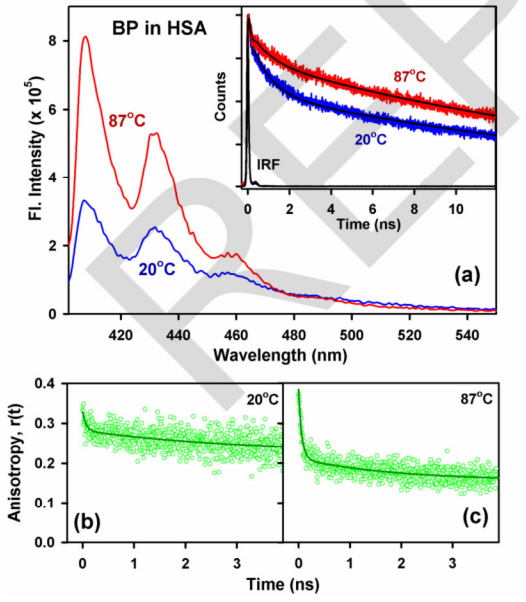

Figs. 18. (a) Fluorescence spectra of BP in HSA at 20° and 87°C and inset shows the corresponding time-resolved fluorescence transients. Fluorescence anisotropy of the same at (b) 20°C and (c) 87°C. Solid lines indicate exponential fitting of the experimental data points. (Reprinted with permission from reference [21]. Copyright 2013, American Chemical Society)

The values of the respective τ_r have been tabulated in Table XII. The fluorescence aniosotropy of BP in CT-DNA at 20°C produces a τ_r value of 140 ps which corresponds to the rotational motion of the probe BP in the DNA, along with a residual offset of 0.15. The origin of such offset is due to the overall motion of the DNA which does not decay within the experimental time window.

Using the time-resolved fluorescence anisotropy study, Ghiggino and co-workers [65] have documented the dynamics of energy transfer in multiporphyrin functionalized dendrimers where they observed a fast decay (~80 ps) in the anisotropy profile with a residual offset similar to our observation. As shown in Figure 17 and Table XII, the rotational time constant of BP in CT-DNA decreases from 140 ps to 70 ps and the residual offset becomes negligible as the DNA reaches its melting temperature.

The τ_r value calculated for BP in CT-DNA at 87°C is close to that calculated for BP in buffer at the same temperature, indicating the release of BP to buffer with the melting of DNA. Here it has to be noted that the solubility of BP in aqueous medium at low temperatures being extremely low, experiments could not be performed with the aqueous solution of BP at low temperatures.

However, the solubility of the same in aqueous buffer medium increases from 10^{-8} M to 10^{-7} M, with enhancement in temperature from 20 to 87^0C. Therefore, with the dilute aqueous solution of BP at 87^0C in 0.05 M phosphate buffer, anisotropy experiments have been performed which gives the rotational time constant of 50 ps without any offset.

The higher solubility of BP in buffer at elevated temperature further supports the release of BP from DNA at the DNA melting temperature around 87°C. Thus, unlike ethidium (Et), a well known DNA intercalator which significantly remains bound to single stranded (ss) DNA upon DNA melting producing a characteristic lifetime component [66] of about 18 ns and a DNA minor groove binder, Hoechst 33258 (H258) which also remains associated with DNA at high temperatures [63], BP almost completely dissociates from DNA at high temperature (beyond the melting temperature of DNA) with no signature of binding to ss DNA.

After investigating ET reaction from BP to CT-DNA in a temperature-dependent manner, we further investigated such interaction with another biological macromolecule, human serum albumin (HSA), as carcinogens are known to interact not only with DNAs but also with Proteins [27], [67]. Figure 18a shows the emission spectra of BP in HSA at 20 and 87°C upon excitation with UVA radiation.

The relatively lower emission intensity of BP at the aggregate peak around 490 nm compared to the monomer peaks at 410, 430 and 455 nm, similar to our observation for BP upon complexation with CT-DNA (Figs 14(a)), is again a clear evidence of association between the carcinogen and HSA.

TABLE XIII
FLUORESCENCE LIFETIME COMPONENTS (τ) OF BP UPON INTERACTION WITH HSA AT DIFFERENT TEMPERATURES ALONG WITH THE ROTATIONAL TIME CONSTANTS (τ_R). EMISSION WAVELENGTH (λ_{Em}) AND EXCITATION WAVELENGTH (λ_{Ex}) ARE 410 AND 375 NM RESPECTIVELY. THE NUMBERS IN PARENTHESIS REPRESENT RELATIVE CONTRIBUTION OF THE COMPONENT. τ_{Av} REPRESENTS THE AVERAGE LIFETIME IN NS. ERROR ±5%

Sample	Temperature (°C)	τ_1 (ns)	τ_2 (ns)	τ_3 (ns)	τ_{av} (ns)	Anisotropy		
						τ_r (ns)		Offset
BP in HSA	20	0.07 (39%)	0.87 (23%)	19.09 (38%)	7.48	0.07 (46%)	2.99 (54%)	0.22
	87	0.07 (37%)	0.90 (13%)	20.12 (50%)	10.20	0.06 (76%)	1.89 (24%)	0.16

As evident from the Fig. 18(a), the emission intensity of BP in the presence of HSA also enhances with the increase in temperature from 20 to 87°C similar to that observed for BP-CT-DNA complex. However, the extent of enhancement in the emission intensity of BP in the presence of HSA is much lower compared to that in the presence of CT-DNA.

Therefore, with the increase in temperature the ET pathway of BP in the presence of HSA gets perturbed to some lower extent, compared to our previous observation in the presence of CT-DNA. Fig. 18(a) inset shows the time-resolved fluorescence transients of BP-HSA complex at 20 and 87°C while exciting with UVA radiation. The corresponding lifetime components have been tabulated in Table XIII.

The ultrafast time components of 70 and 870 ps in the lifetime of BP upon association with HSA strongly corroborate with the ET components observed in the fluorescence transients of BP while participating in ET reaction with BQ and DNA, mentioned above and thus have been attributed to the UVA radiation induced ET from BP to HSA.

Amino acids in HSA possessing lower oxidation potential compared to BP can be involved in such ET reaction from BP to HSA. For example, the oxidation potential of tryptophan in HSA being lower (~1 V) [68] than that of BP (~1.18 V) [69], supports the flow of electrons from BP to HSA in the observed ET reaction between the two. In contrast to our previous observation in the presence of CT-DNA, the contribution of ET components of 70 and 870 ps in the fluorescence transient of BP in the presence of HSA found to get decreased from 39 to 37% and from 23 to 13%, respectively, with the similar increase in temperature from 20 to 87°C.

The major contribution of the ET components in the fluorescence transient of BP in HSA even at 87°C, where the protein gets significantly unfolded [70], suggests that BP remains bound to unfolded HSA unlike CT-DNA at high temperature. For further confirmation regarding the association of BP with unfolded HSA, the fluorescence anisotropy of BP at 87°C has been compared with that at 20°C as shown in Figures 18(b) and (c). At both the temperatures 20 and 87°C, the anisotropy exhibits biexponential decay with a residual offset of 0.22 and 0.16, respectively. The corresponding τ_r values are tabulated in Table XIII.

The offset observed in BP-HSA complex at 20°C and 87°C is due to the overall motion of the protein HSA which does not decay within the experimental time window.

The ultrafast time component ~70 ps with a huge offset, observed in the temporal decays of the rotational anisotropy of BP bound to HSA at 20 and 87°C, is comparable to the electronic energy transfer component in the anisotropy profile of multiporphyrin functionalized dendrimers [65] mentioned before.

The presence of electronic energy transfer component along with a significant residual offset in the rotational anisotropy of BP in unfolded HSA at 87°C confirm the association of BP with unfolded HSA unlike denatured CT-DNA. The association of BP with unfolded HSA strongly corroborates with one of our earlier studies[70], where it has been shown that an extremely hydrophobic probe can reside in the subdomain IIIA of the protein even at its thermally unfolded states.

III.2.3. Investigation on the ET Reaction from BP to Zinc Oxide (ZnO) Nanorods (NRs)

Our investigation on the ET reaction from BP to organic molecules and biological macromolecules (shown in Scheme 1a and b) has been further extended with inorganic zinc oxide (ZnO) nanorods (NRs). The purpose of this study is to probe whether ET from BP to ZnO NRs is achieved in terms of photocurrent. By making the use of basic working principle of a dye-sensitized solar cell, we have designed a photodevice, as schematically shown in Scheme 1(c). Fig. 19(a) left inset shows the scanning electron micrographs (SEM images) of ZnO NRs. Morphological characterization by SEM (Figure 19(a) left inset) indicates the formation of arrays of ZnO NRs with a preferential growth along the polar facets [002 direction] of the hexagonal wurtzite crystal.

The NRs growing perpendicular to the substrate are nearly uniform in length (~3 μm) and possess a characteristic hexagonal cross-section with diameter in the range of 180 nm.

For the investigation of UVA radiation induced ET reaction between BP monomers and ZnO NRs, picosecond-resolved fluorescence transient of BP has been monitored at 410 nm on thin film in the presence of ZnO NRs as shown in Fig. 19(a) and it is fitted with the values given in Table XIV.

TABLE XIV
THE LIFETIME COMPONENTS OF BP MONITORED AT 410 nm (λ_{em}) ON THIN FILM IN PRESENCE OF ZnO NRs. τ REPRESENTS THE TIME CONSTANT IN ns AND THE NUMBERS IN THE PARENTHESIS REPRESENT RELATIVE CONTRIBUTION OF THE COMPONENTS. ERROR ±5%

Sample	τ_1 (ns)	τ_2 (ns)	τ_3 (ns)
ZnO NR anchored BP	0.05 (89%)	0.88 (6%)	39.64 (5%)

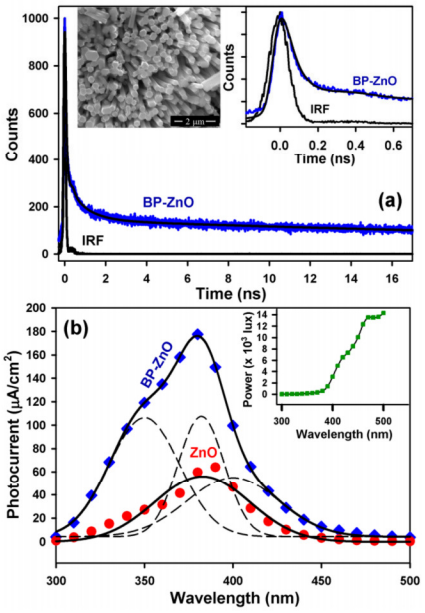

Figs. 19. (a) The time-resolved fluorescence transient of BP-ZnO complex in thin film and the right inset shows the same in a narrow time window, the left inset shows the scanning electron micrographs (SEM images) of ZnO NRs, (b) the wavelength-dependent photocurrent obtained from ZnO NR fabricated photodevices in the presence and absence of BP. Bold lines represent the Gaussian fits of the respective plots and the broken lines represent the deconvoluted plots of BP-ZnO complex having peaks at 350, 382 and 400 nm. Inset shows the variation of power over the same wavelength range where the bold line is the guide to the eye. (Reprinted with permission from reference [21]. Copyright 2013, American Chemical Society)

As evident from Fig. 19(a) and Table XIV, ultrafast components of 50 and 880 ps appear in the fluorescence transient of BP in presence of ZnO NRs, along with a long component (~39 ns) comparable to the lifetime of BP in degassed benzene[26]. To differentiate the ultrafast component of 50 ps from IRF, the fluorescence transient of ZnO NR anchored BP is shown over a narrow time window of 0.7 ns in Fig. 19(a) right inset.

The ultrafast components in the fluorescence transient of BP in the presence of ZnO NRs being comparable with the ET components observed in the fluorescence transients of the same while undergoing ET reaction with organic molecules and biological macromolecules (mentioned before) validate the ET from BP to ZnO NRs.

Here it has to be noted that the observed ET components in the lifetime of BP in different systems are similar but they are exactly not the same and this difference can be attributed to the difference in redox properties of the systems. Moreover the picosecond resolved lifetime measurements were all done in time correlated single photon counting (TCSPC) setup having instrument response function (IRF) of 80 ps hence very fine variations (in femtosecond time scale) of the ET process are beyond the resolution of the used setup. The ET from BP to ZnO NRs has been further confirmed by monitoring the flow of electrons in terms of photocurrent.

Fig. 19(b) shows the wavelength dependent variation in photocurrent, monitored in ZnO NR fabricated photodevice in the presence and absence of BP. As shown by the broken lines in the Figure 19b, the photocurrent vs. wavelength curve in the presence of BP can be deconvoluted into three characteristic peaks at 350, 382 and 400 nm similar to the absorption peaks of BP [52] while that in absence of BP produces a single peak corresponding to the absorption peak of ZnO at 382 nm. The enhanced photocurrent obtained in the presence of BP from ZnO NR fabricated photodevice confirms the role of BP as the photosensitizer.

Inset of Fig. 19(b) indicates that in the wavelength range of 300 to 380 nm, power remains almost constant while there is a constant enhancement in photocurrent, suggesting that the photocurrent measured is solely dependent on the flow of electrons irrespective of the power.

IV. Conclusion

In the present review we have discussed the effect of excited state lifetime of a well known biological probe and food carcinogen benzo[*a*]pyrene (BP) in various solvents of different degrees polarity/proticity/dielectric constants and polarizabilities.

Although the steady-state spectral shift is expected to follow the theoretical models, the time resolved studies on a number of solvents clearly invite better theoretical understanding of the photophysics of BP. Our present study also highlights the importance of the consideration of differential spectral overlap of the vibronic bands of BP undergoing FRET as a consequence of dipole-dipole interaction with an organic molecule in a confined environment.

The differential behavior of the vibronic bands of BP under FRET has been compared with the behavior of a dye molecule in a dye-blend under FRET which shows reasonable similarity. Finally we have shown that the differential $J(\lambda)$ analysis is equally acceptable to the standard theoretical frame work for further interpretation of FRET data including the Infelta-Tachiya model and P(r) analysis techniques.

Our reported studies may find importance in the FRET analysis of biologically relevant pyrene class of molecules. Besides emphasizing the characteristic property of the carcinogenic pyrene derivative while undergoing energy transfer reaction with other molecules in a biologically relevant environment, we have discussed the strong affinity of the carcinogen BP to donate electrons to different class of molecules like para-benzoquinone (BQ), biological macromolecules like calf-thymus DNA and human serum albumin (HSA) and inorganic nano structures like zinc oxide (ZnO) nanorods (NRs). While steady state and time resolved fluorescence spectroscopy results reveal the quenching of the emission of BP in presence of organic molecules, biological macromolecules and nano structures, CD spectroscopy results monitor the BP induced structural changes in the

CT-DNA and ZnO-NR based photodevice confirm the charge transfer reaction from BP by directly monitoring the flow of electrons in terms of photocurrent.

Our ultrafast electron transfer studies from BP to four different types of molecules suggest BP as a strong electron donor which can be considered as one of its vital characteristics responsible for its carcinogenic activity.

Therefore, our study hints that the ET pathway from BP can be targeted to prevent BP mediated carcinogenesis. It has to be noted that carcinogenesis of BP may involve other modes of interaction with biological macromolecules apart from ET which our review does not include. We emphasize one of the key aspects of BP which can assist in further research on this carcinogen.

Acknowledgements

S. B thanks UGC India and S.C thanks CSIR India, for providing research fellowships. We thank DST, India, for financial grant (DST/TM/SERI/2k11/103 and SB/SI/PC-011/2013). We thank colleagues in our laboratory at S.N. Bose National Centre for Basic Sciences, whose contributions over the years, acknowledged in the references, have been priceless in the successful evolution of work in this area. In particular, we thank Mr. Nirmal Goswami and Mr. Soumik Sarkar.

We thank Prof. Joydeep Dutta and Mr. Karthik Lakshman, Water Research Center, Sultan Qaboos University, Muscat, Oman and Prof Masanori Tachiya, Advanced Industrial Science and Technology (AIST), Tsukuba (Japan) for the collaborative works.

References

[1] Gratzel, M., Thomas, J. K., On the Dynamics of Pyrene Fluorescence Quenching in Aqueous Ionic Micellar Systems. Factors Affecting the Permeability of Micelles, *J. Am. Chem. Soc.*, *volume 95,* (issue 21), *October 1973*, *pages 6885-6889*.

[2] Kalyanasundaram, K., Thomas, J. K., Environmental Effects on Vibronic Band Intensities in Pyrene Monomer Fluorescence and Their Application in Studies of Micellar Systems, *J. Am. Chem. Soc.*, *volume 99,* (issue 7), *March 1977*, *pages 2039-2044*.

[3] Morrisett, J. D., Pownall, H. J. *et al.*, Multiple Thermotropic Phase Transitions in Escherichia coli Membranes and Membrane Lipids. A comparison of Results Obtained by Nitroxyl Stearate Paramagnetic Resonance, Pyrene Excimer Fluorescence, and Enzyme Activity Measurements, *J. Biol. Chem.*, *volume 250,* (issue 17), *September 1975*, *pages 6969-6976*.

[4] Sigalat, J. A., SanMartin, J. S. *et al.*, Further Insight into the Photostability of the Pyrene Fluorophore in Halogenated Solvents, *ChemPhysChem*, *volume 13,* (issue 3), *February 2012*, *pages 835-844*.

[5] Shyamala, T., Sankararaman, S. *et al.*, 1,3,6,8-Tetraethynylpyrene and 1,3,6,8-tetrakis (trimethylsilylethynyl) pyrene: Photophysical Properties in Homogeneous Media, *Chem. Phys.*, *volume 330,* (issue 3), *November 2006*, *pages 469-477*.

[6] Beck, S. C., Cramb, D. T., Condensed Phase Dispersive Interactions of Benzo[a]pyrene with Various Solvents and with DNA: A Twist on Solvatochromism, *J. Phys. Chem. B*, *volume 104,* (issue 12), *March 2000*, *pages 2767-2774*.

[7] Vigil, M. R., Bravo, J. *et al.*, Photochemical Sensing of Semicrystalline Morphology in Polymers: Pyrene in Polyethylene, *Macromolecules*, *volume 30,* (issue 17), *August 1997*, *pages 4871-4876*.

[8] Hsu, G. W., Huang, X. *et al.*, Structure of a High Fidelity DNA Polymerase Bound to a Benzo[a]pyrene Adduct That Blocks Replication, *J. Biol. Chem.*, *volume 280,* (issue 5), *February 2005*, *pages 3764-3770*.

[9] Dutta, K., Ghosh, D. *et al.*, A Common Carcinogen Benzo[a]pyrene Causes Neuronal Death in Mouse via Microglial Activation, *Plos one*, *volume 5,* (issue 4), *April 2010*, *pages 1-14*.

[10] Kometania, T., Yoshinob, I. *et al.*, Benzo[a]pyrene Promotes Proliferation of Human Lung Cancer Cells by Accelerating the Epidermal Growth Factor Receptor Signaling Pathway, *Cancer Lett.*, *volume 278,* (issue 1), *June 2009*, *pages 27-33*.

[11] Hongjing Tian, Qingjie Guo, Investigation into the Reactivity of Calcium Sulfate with Gaseous and Solid Fuels and Thermodynamic Analysis of Carbon Deposits and Sulfur Evolution in Chemical-looping Combustion System, (2009) *International Review of Chemical Engineering (IRECHE),* 1. (1), pp. 51-57.

[12] Raul G. Bautista-Margulis, Jose R. Hernandez-Barajas, Ruben A. Saucedo-Teran, Combustion of Coal Volatiles in the Freeboard of a Fluidized Bed Combustor: an Experimental Approach, (2009) *International Review of Chemical Engineering (IRECHE),* 1. (1), pp. 58-65.

[13] Schuler, B., Lipman, E. A. *et al.*, Polyproline and the ''Spectroscopic Ruler'' Revisited with Single-Molecule Fluorescence, *Proc. Natl. Acad. Sci.*, *volume 102,* (issue 8), *February 2005*, *pages 2754-2759*.

[14] Shaw, A. K., Sarkar, R. *et al.*, Direct Observation of DNA Condensation in a Nano-Cage by Using a Molecular Ruler, *Chem. Phys. Lett.*, *volume 408,* (issue 4-6), *June 2005*, *pages 366-370*.

[15] Clapp, A. R., Medintz, I. L. *et al.*, Förster Resonance Energy Transfer Investigations Using Quantum-Dot Fluorophores, *ChemPhysChem*, *volume 7,* (issue 1), *January 2006*, *pages 47-57*.

[16] Banerjee, D., Pal, S. K., Simultaneous Binding of Minor Groove Binder and Intercalator to Dodecamer DNA: Importance of Relative Orientation of Donor and Acceptor in FRET, *J. Phys. Chem. B*, *volume 111,* (issue 19), *April 2007*, *pages 5047-5052*.

[17] Chen, F. M., Binding of Pyrene to DNA, Base Sequence Specificity and its Implication, *Nucleic Acids Res.*, *volume 11,* (issue 20), *October 1983*, *pages 7231-7250*.

[18] Masuko, M., Ohuchi, S. *et al.*, Fluorescence Resonance Energy Transfer from Pyrene to Perylene Labels for Nucleic Acid Hybridization Assays under Homogeneous Solution Conditions, *Nucleic Acids Res.*, *volume 28,* (issue 8), *April 2000*, *pages e34i-viii*.

[19] Kupstat, A., Knopp, D. *et al.*, Novel Intramolecular Energy Transfer Probe for the Detection of Benzo[a]pyrene Metabolites in a Homogeneous Competitive Fluorescence Immunoassay, *J. Phys. Chem. B*, *volume 114,* (issue 4), *January 2010*, *pages 1666-1673*.

[20] Majumder, P., Sarkar, R. *et al.*, Ultrafast Dynamics in a Nanocage of Enzymes: Solvation and Fluorescence Resonance Energy Transfer in Reverse Micelles, *J. Colloid Interface Sci.*, *volume 290,* (issue 2), *October 2005*, *pages 462-474*.

[21] Banerjee, S., Sarkar, S. *et al.*, UVA Radiation Induced Ultrafast Electron Transfer from a Food Carcinogen Benzo[a]pyrene to Organic Molecules, Biological Macromolecules and Inorganic Nano Structures, *J. Phys. Chem. B*, *volume 117,* (issue 14), *March 2013*, *pages 3726-3737*.

[22] Eling, T. E., Thompson, D. C. *et al.*, Prostaglandin H Synthase and Xenobiotic Oxidation, *Annu. Rev. Pharmacol. Toxicol.*, *volume 30,* (issue April), *1990*, *pages 1-45*.

[23] Wilk, M., Girke, W., Reactions Between Benzo[a]pyrene and Nucleo Bases by One-Electron Oxidation, *J. Natl. Cancer Inst.*, *volume 49,* (issue 6), *August 1972*, *pages 1585-5197*.

[24] Wan, C., Fiebig, T. *et al.*, Femtosecond Dynamics of DNA-Mediated Electron Transfer, *Proc. Natl. Acad. Sci.*, *volume 96,* (issue 11), *May 1999*, *pages 6014-6019*.

[25] Nguyena, J., Maa, Y. *et al.*, Direct Observation of Ultrafast-Electron-Transfer Reactions Unravels High Effectiveness of Reductive DNA Damage, *Proc. Natl. Acad. Sci.*, *volume 108,* (issue 29), *July 2011*, *pages 11778-11783*.

[26] Geacintov, N. E., Prusik, T. *et al.*, Properties of Benzopyrene-DNA Complexes Investigated by Fluorescence and Triplet Flash Photolysis Techniques, *J. Am. Chem. Soc.*, *volume 98,* (issue 21),

October 1976, *pages 6444-6452*.

[27] Skipper, P. L., Tannenbaum, S. R., Protein Adducts in the Molecular Dosimetry of Chemical Carcinogens, *Carcinogenesis*, *volume 11,* (issue 4), *April 1990*, *pages 507-518*.

[28] Kure, E. H., Andreassen, A. *et al.*, Benzo(a)pyrene-Albumin Adducts in Humans Exposed to Polycyclic Aromatic Hydrocarbons in an Industrial Area of Poland, *Occup. Environ. Med.*, *volume 54,* (issue 9), *September 1997*, *pages 662-666*.

[29] Srinivasan, B. N., Fujimori, E., Benzo[a]pyrene-Serum: Albumin/Cysteine Interactions: Fluorescene and Electron Spin Resonance Studies, *Chem. Biol. Interact.*, *volume 28,* (issue 1), *November 1979*, *pages 1-15*.

[30] Brenner, D. J., Doll, R. *et al.*, Cancer Risks Attributable to Low doses of Ionizing radiation: Assessing What We Really Know, *Proc. Natl. Acad. Sci.*, *volume 100,* (issue 24), *November 2003*, *pages 13761-13766*.

[31] Land, C. E., Boice, J. D. *et al.*, Breast Cancer Risk From Low-Dose Exposures to Ionizing Radiation: Results of Parallel Analysis of Three Exposed Populations of Women, *J. Natl. Cancer Inst.*, *volume 65,* (issue 2), *February 1980*, *pages 353-376*.

[32] Kawanishi, S., Hiraku, Y. *et al.*, Mechanism of Guanine-Specific DNA Damage by Oxidative Stress and its Role in Carcinogenesis and Aging, *Mutat. Res. Rev. Mutat.* , *volume 488,* (issue 1), *March 2001*, *pages 65-76*.

[33] Toyooka, T., Ibuki, Y. *et al.*, Coexposure to Benzo[a]pyrene Plus UVA Induced DNA Double Strand Breaks: Visualization of Ku Assembly in the Nucleus Having DNA Lesions, *Biochem. Biophys. Res. Commun.*, *volume 322,* (issue 2), *September 2004*, *pages 631-636*.

[34] Toyooka, T., Ibuki, Y. *et al.*, Coexposure to Benzo[a]pyrene and UVA Induces DNA Damage: First proof of Double-Strand Breaks in a Cell-Free System, *Environ. Mol. Mutagen.*, *volume 47,* (issue 1), *January 2006*, *pages 38-47*.

[35] Kang, Q., Chen, Y. *et al.*, A Photoelectrochemical Immunosensor for Benzo[a]pyrene Detection Amplified by Bifunctional Gold Nanoparticles, *Chem. Commun.*, *volume 47,* (issue 46), *December 2011*, *pages 12509-12511*.

[36] Alexandrova, K., Dragieva, I. *et al.*, Preparation and Characterization of Nickel Nanoparticles and Nanowires in Aqueous Solution Under Wet Chemical Process, *Int. Review of Chem. Engineering*, *volume 1,* (issue 2), *March 2009*, *pages 206-211*.

[37] Lakowicz, J. R. *Principles of Fluorescence Spectroscopy*; Kluwer Academic/Plenum: New York, 1999.

[38] Goswami, N., Makhal, A. *et al.*, Toward an Alternative Intrinsic Probe for Spectroscopic Characterization of a Protein, *J. Phys. Chem. B*, *volume 114,* (issue 46), *October 2010*, *pages 15236-15243*.

[39] Banerjee, S., Tachiya, M. *et al.*, Caffeine-Mediated Detachment of Mutagenic Ethidium from Various Nanoscopic Micelles: An Ultrafast Förster Resonance Energy Transfer Study, *J. Phys. Chem. B*, *volume 116,* (issue 27), *June 2012*, *pages 7841-7848*.

[40] Tachiya, M., Application of a Generating Function to Reaction Kinetics in Micelles. Kinetics of Quenching of Luminescent Probes in Micelles, *Chem. Phys. Lett.*, *volume 33,* (issue 2), *June 1975*, *pages 289-292*.

[41] Sadhu, S., Tachiya, M. *et al.*, A Stochastic Model for Energy Transfer from CdS Quantum Dots/Rods (Donors) to Nile Red Dye (Acceptors), *J. Phys. Chem. C*, *volume 113,* (issue 45), *October 2009*, *pages 19488-19492*.

[42] Batabyal, S., Mondol, T. *et al.*, Picosecond-Resolved Solvent Reorganization and Energy Transfer in Biological and Model Cavities, *Biochimie*, *volume 95,* (issue 6), *June 2013*, *pages 1127-1135*.

[43] Sarkar, S., Makhal, A. *et al.*, Hematoporphyrin–ZnO Nanohybrids: Twin Applications in Efficient Visible-Light Photocatalysis and Dye-Sensitized Solar Cells, *ACS Appl. Mater. Interfaces*, *volume 4,* (issue 12), *November 2012*, *pages 7027-7035*.

[44] Sarkar, S., Makhal, A. *et al.*, Dual-Sensitization via Electron and Energy Harvesting in CdTe Quantum Dots Decorated ZnO Nanorod-Based Dye-Sensitized Solar Cells, *J. Phys. Chem. C*, *volume 116,* (issue 27), *June 2012*, *pages 14248-14256*.

[45] Tanumoy Mondol, Soma Banerjee, Subrata Batabyal, Samir Kumar Pal, Study of Biomolecular Recognition Using Time-resolved Optical Spectroscopy, (2011) *International Review of Biophysical Chemistry (IREBIC),* 2 (6), pp. 211-237.

[46] Mahler, H. R., Perlman, P. S., Effects of Mutagenic Treatment by Ethidium Bromide on Cellular and Mitochondrial Phenotype, *Arch. Biochem. Biophys.*, *volume 148,* (issue 1), *January 1972*, *pages 115-129*.

[47] Pal, S. K., Mandal, D. *et al.*, Photophysical Processes of Ethidium Bromide in Micelles and Reverse Micelles, *J. Phys. Chem. B*, *volume 102,* (issue 52), *December 1998*, *pages 11017-11023*.

[48] Revillod, G., Antoine, I. R. *et al.*, Investigating the Interaction of Crystal Violet Probe Molecules on Sodium Dodecyl Sulfate Micelles with Hyper-Rayleigh Scattering, *J. Phys. Chem. B*, *volume 109,* (issue 11), *February 2005*, *pages 5383-5387*.

[49] Soma Banerjee, Samir Kumar Pal, Caffeine Mediated Dissociation of a Potential Mutagen from DNA Mimetics, DNA and Cellular Nuclei: Ultrafast Spectroscopic Studies, (2012) *International Review of Biophysical Chemistry (IREBIC),* 3 (6), pp. 173-204.

[50] Banerjee, S., Goswami, N. *et al.*, A Potential Carcinogenic Pyrene Derivative under Forster Resonance Energy Transfer to Various Energy Acceptors in Nanoscopic Environments, *ChemPhysChem*, *volume 14,* (issue 15), *October 2013*, *pages 3581-3593*.

[51] Ogilby, P. R., Solvent Effects on the Radiative Transitions of Singlet Oxygen, *Acc. Chem. Res.*, *volume 32,* (issue 6), *February 1999*, *pages 512-519*.

[52] Larsen, J. S., Waluk, J. *et al.*, Electronic States of Benzo[a]pyrene. Linear and Magnetic Circular Dichroism, Polarized Fluorescence, and Quantum Chemical Calculations, *J. Am. Chem. Soc.*, *volume 114,* (issue 6), *March 1992*, *pages 1942-1949*.

[53] Gritsan, N. P., Pritchina, E. A. *et al.*, Excited-State Dynamics in the Covalently Linked Systems: Pyrene-(CH_2) n -Aryl Azide, *J. Phys. Chem. C*, *volume 113,* (issue 27), *April 2009*, *pages 11579-11589*.

[54] Shaw, A. K., Pal, S. K., Fluorescence Relaxation Dynamics of Acridine Orange in Nanosized Micellar Systems and DNA, *J. Phys. Chem. B*, *volume 111,* (issue 16), *March 2007*, *pages 4189-4199*.

[55] Park, J. W., Chung, H., Aggregation and Dissolution of Cationic Dyes with an Anionic Surfactant, *Bull. Korean. Chem. Soc.*, *volume 7,* (issue 2), *April 1986*, *pages 113-116*.

[56] Wiosetek-Reske, A. M., Wysocki, S., Spectral Studies of N-nonyl Acridine Orange in Anionic, Cationic and Neutral Surfactants, *Spectrochim. Acta A*, *volume 64,* (issue 5), *August 2006*, *pages 1118-1124*.

[57] Atal, N., Saradhi, P. P. *et al.*, Inhibition of the Chloroplast Photochemical Reactions by Treatment of Wheat Seedlings with Low Concentrations of Cadmium: Analysis of Electron Transport Activities and Changes in Fluorescence Yield *Plant Cell Physiol.*, *volume 32,* (issue 7), *October 1991*, *pages 943-951*.

[58] Cooper, C. D., Naff, W. T. *et al.*, Negative Ion Properties of p-Benzoquinone: Electron Affinity and Compound States, *J. Chem. Phys.*, *volume 63,* (issue 6), *September 1975*, *pages 2752-2757*.

[59] Wells, T. A., Losi, A. *et al.*, Electron Transfer Quenching and Photoinduced EPR of Hypericin and the Ciliate Photoreceptor Stentorin, *J. Phys. Chem. A*, *volume 101,* (issue 4), *January 1997*, *pages 366-372*.

[60] Leland, B. A., Joran, A. D. *et al.*, Picosecond Fluorescence Studies on Intramolecular Photochemical Electron Transfer in Porphyrins Linked to Quinones at Two Different Fixed Distances, *J. Phys. Chem.*, *volume 89,* (issue 26), *December 1985*, *pages 5571-5573*.

[61] Chen, G., Cooks, R. G., Electron Affinities of Polycyclic Aromatic Hydrocarbons Determined by the Kinetic Method, *J. Mass. Spectrom.*, *volume 30,* (issue 8), *August 1995*, *pages 1167–1173*.

[62] Sutherland, J. C., Griffin, K. P., Absorption Spectrum of DNA for Wavelengths Greater Than 300 nm, *Rad. Res.*, *volume 86,* (issue 3), *June 1981*, *pages 399-410*.

[63] Banerjee, D., Pal, S. K., Direct Observation of Essential DNA Dynamics: Melting and Reformation of the DNA Minor Groove, *J. Phys. Chem. B*, *volume 111,* (issue 36), *August 2007*, *pages*

10833-10838.
[64] Douki, T., Effect of Denaturation on the Photochemistry of Pyrimidine Bases in Isolated DNA, *J. Photochem. Photobiol. B*, *volume 82,* (issue 1,2), *January 2006*, *pages 45-52*.
[65] Yeow, E. K. L., Ghiggino, K. P. *et al.*, The Dynamics of Electronic Energy Transfer in Novel Multiporphyrin Functionalized Dendrimers: A Time-Resolved Fluorescence Anisotropy Study, *J. Phys. Chem. B*, *volume 104,* (issue 12), *March 2000*, *pages 2596-2606*.
[66] Banerjee, S., Bhowmik, D. *et al.*, Ultrafast Spectroscopic Study on Caffeine Mediated Dissociation of Mutagenic Ethidium from Synthetic DNA and Various Cell Nuclei, *J. Phys. Chem. B*, *volume 115,* (issue 49), *October 2011*, *pages 14776-14783*.
[67] Ketterer, B., Interactions Between Carcinogens and Proteins, *Br. Med. Bull.*, *volume 36,* (issue 1), *January 1980*, *pages 71-78*.
[68] Marme, N., Knemeyer, J. P. *et al.*, Inter- and Intramolecular Fluorescence Quenching of Organic Dyes by Tryptophan, *Bioconjugate Chem.*, *volume 14,* (issue 6), *November 2003*, *pages 1133-1139*.
[69] Keskin, E., Yardım, Y. *et al.*, Voltammetry of Benzo[a]pyrene in Aqueous and Nonaqueous Media: Adsorptive Stripping Voltammetric Determination at Pencil Graphite Electrode, *Electroanalysis*, *volume 22,* (issue 11), *June 2010*, *pages 1191-1199*.
[70] Sinha, S. S., Mitra, R. K. *et al.*, Temperature-Dependent Simultaneous Ligand Binding in Human Serum Albumin, *J. Phys. Chem. B*, *volume 112,* (issue 16), *April 2008*, *pages 4884-4891*.

Authors' information

Department of Chemical, Biological & Macromolecular Sciences,S. N. Bose National Centre for Basic Sciences, Block JD, Sector III, Salt Lake, Kolkata 700 098, India.
E-mail: skpal@bose.res.in

Soma Banerjee was born (1986) in Kolkata, India. Upon accomplishing her B.Sc. (2007) and M.Sc. (2009) degrees in biochemistry, both from the Calcutta University, Kolkata (India), she joined Ph.D. under the supervision of Prof. Samir Kumar Pal at S. N. Bose National Centre for Basic Sciences, Kolkata, India. The focus of her current study is the exploration of biomolecular recognition of medicinally important ligands including some plant alkaloids involving ultrafast spectroscopy.

Siddhi Chaudhuri was born (1985) in Kolkata, India. Upon accomplishing her B.Sc. (2007) and M.Sc. (2009) degrees in biochemistry, both from the Calcutta University, Kolkata (India), she joined Ph.D. under the supervision of Prof. Samir Kumar Pal at S. N. Bose National Centre for Basic Sciences, Kolkata, India. The focus of her research is to study the conjugation of medicinally important drugs with various nanoparticles in order enhance their bioavailability using spectroscopic methods.

Samir Kumar Pal is presently professor in the Department of Chemical Biological and Macromolecular Sciences, S. N. Bose National Centre for Basic Sciences, Kolkata, India. He is also one of the investigators in the unit for Nano Science and Technology of the Centre (WWW: http://www.bose.res.in/faculty/skpal.htm).

